Journal of Medicinal Chemistry

Article

Design, Synthesis, and Evaluation of Novel p-(methylthio)styryl Substituted Quindoline Derivatives as Neuroblastoma RAS (NRAS) Repressors via Specific Stabilizing the RNA G-Quadruplex

Wang Peng, Zhi-Yin Sun, Qi Zhang, Sui-Qi Cheng, Shi-Ke Wang, Xiao-Na Wang, Guo-Tao Kuang, Xiao-Xuan Su, Jia-Heng Tan, Zhi-Shu Huang, and Tian-Miao Ou

J. Med. Chem., **Just Accepted Manuscript** • DOI: 10.1021/acs.jmedchem.8b00257 • Publication Date (Web): 25 May 2018

ACS Publications

is published by the American Chemical Society. 1155 Sixteenth Street N.W., Washington, DC 20036

Design, Synthesis, and Evaluation of Novel *p*-(methylthio)styryl Substituted Quindoline Derivatives as Neuroblastoma RAS (NRAS) Repressors via Specific Stabilizing the RNA G-Quadruplex

Wang Peng, Zhi-Yin Sun, Qi Zhang, Sui-Qi Cheng, Shi-Ke Wang, Xiao-Na Wang, Guo-Tao Kuang, Xiao-Xuan Su, Jia-Heng Tan, Zhi-Shu Huang, Tian-Miao Ou*

School of Pharmaceutical Sciences, Sun Yat-sen University, Guangzhou 510006, P. R. China.

ABSTRACT

The human proto-oncogene neuroblastoma *RAS* (*NRAS)* contains a guanine-rich sequence in the 5'-untranslated regions (5'-UTR) of the mRNA that could form an RNA G-quadruplex structure. This structure acts as a repressor for *NRAS* translation and could be a potential target for anti-cancer drugs. Our previous studies found an effective scaffold, the quindoline scaffold, for binding and stabilizing the DNA G-quadruplex structures. Here, basing on the previous studies and reported RNA-specific probes, a series of novel *p*-(methylthio)styryl substituted quindoline (**MSQ**) derivatives were designed, synthesized and evaluated as *NRAS* RNA G-quadruplex ligands. Panels of experiments turned out that the introduction of *p*-(methylthio)styryl side chain could enhance the specific binding to the *NRAS* RNA G-quadruplex. One of the hits, **4a-10**, showed strong stabilizing activity on the G-quadruplex, and subsequently repressed *NRAS*'s translation and inhibited tumor cells proliferation. Our finding provided a novel strategy to discover novel *NRAS* repressors by specifically binding to the RNA G-quadruplex in the 5'-UTR of mRNA.

KEWORDS

NRAS RNA G-quadruplex; *p*-(methylthio)styryl substituted quindoline derivatives; translational repressor; anti-tumor

■ INTRODUCTION

The neuroblastoma RAS (*NRAS*) viral oncogene homolog belongs to the *RAS* gene family, which is a well-studied human oncogene family encoding a RAS superfamily. Proteins in the RAS superfamily are mainly monomeric small (20-25 kDa) guanosine triphosphate (GTP)-binding proteins.[1-2] The RAS proteins play a crucial role in diverse cellular processes (such as proliferation, survival, and differentiation) by regulating the alternation between an active GTP-bound and an inactive guanosine diphosphate (GDP)-bound state in the GTPases.[3] The switch between the states is related to the activation of cell surface receptors within a wide variety of cellular processes thereby leading to the control of proliferation, apoptosis and differentiation.[2, 4-5] Furthermore, RAS proteins interfere with the metabolism of tumor cells, microenvironment's remodeling, evasion of the immune response, and finally contributes to the metastatic process.[6] One third of all human cancers harbors oncogenic mutations in codons 12, 13, or 61 of RAS gene approximately.[1, 7-8] The mutations can produce a protein that binds to GTP more tightly and then disrupts the GTP-to-GDP hydrolysis regulated by a GTP activating protein (GAP), which means the 'on' state of the protein is locked and an over-activation in the downstream pathways.[9-10] Several strategies on developing RAS inhibitors are raised, however, there still no drugs targeting *NRAS* gene due to its multiple mutations.[6]

According to recent reports, there exists a G-rich sequence (5'-GGGAGGGGCGGGUCUGGG-3') in the 5'-untranslated region (5'-UTR) of

human *NRAS* proto-oncogene mRNA, which could form a parallel RNA G-quadruplex structure.[11] The location of this G-rich sequence is 14-nt downstream of the 5'-cap and 222-nt upstream of the translation start site (TSS). Several reports reveal that the RNA G-quadruplex modulates *NRAS*'s translation.[12-13] What's more, the translation of *NRAS* gene can be inhibited by some G-quadruplex ligands.[14-16] This indicates targeting *NRAS* RNA G-quadruplex may be an alternative strategy for discovering of novel *NRAS* repressors as anti-cancer agents.

Stabilizing the G-quadruplex structures in the key regulation regions of oncogenes seems to be an attractive novel anti-tumor strategy and several kinds of G-quadruplex ligands are reported.[17-22] In the previous studies, the quindoline derivatives (**Figure 1**) have been developed as good DNA G-quadruplex binders.[23-29] *In vitro* and *in vivo* studies showed that these quindoline derivatives specifically stabilize the DNA G-quadruplexes in different oncogenes[24, 26, 29-31] or the telomere[23, 25, 28], and exhibit certain antitumor activities.[30-31] The modification strategies are mainly focusing on improving the planarity and aromaticity of the quindoline scaffold to enhance the π-π stacking interactions with the G-quartet, introduction of one or two amino side chains to enhance the hydrogen-bonding interaction and electrostatic binding[28, 30-31], or introduction of a positive charge by methylation at the 5-N position to displace the cation in the central ion channel thereby eliciting stabilizing properties.[25] However, none of these ligands are found to interact with the RNA G-quadruplexes. Besides, few information could be found on structural modification for specific RNA G-quadruplex ligands. Herein, we attempted to modify the

quindoline derivatives to find novel RNA G-quadruplexes ligands.

The styryl group have attracted extensive interest in chemical probe design, and compounds containing the group exhibiting selective binding abilities to RNAs.[32-38] Among these styryl-containing probes, we found the *p*-(methylthio)styryl group can discriminate dsDNAs and RNAs.[34, 39] In order to improve the binding affinity and selectivity to RNA G-quadruplex, we tried to introduce the *p*-(methylthio)styryl group as a side chain to the quindoline scaffold and obtain the novel *p*-(methylthio)styryl substituted quindoline (**MSQ**) derivatives. On the other hand, side chains containing amino, heterocyclic ring, and benzene ring were also introduced at the 11-position; the 5-N position was methylated to enhance the binding affinity according to our previous modification experience (**Figure 1**).

44 **MSQ** compounds were synthesized and their binding affinities with the *NRAS* RNA G-quadruplex and inhibitory activities on tumor cells proliferation were evaluated. We found the introduction of *p*-(methylthio)styryl at 2-position could significantly improve the binding affinity and selectivity to *NRAS* RNA G-quadruplex. We picked out compound **4a-10** from these compounds to further evaluate its inhibitory activity on *NRAS* expression and related events in tumor cells. All the data indicated that **4a-10** can inhibit *NRAS*'s translation via its interaction with *NRAS* RNA G-quadruplex, and interrupting the binding of a helicase, DEAH (Asp-Glu-Ala-His) box polypeptide 36 (DHX36), to this region.

■ RESULTS AND DISCUSSION

Chemistry. The synthetic route for the compounds was shown in **Scheme 1**. The intermediates, **1a-1**, **1a-2**, **1b-1**, and **1b-2**, and *p*-(methylthio) styrene were prepared following the procedures previously reported.[40-42] Intermediates **2a-1**, **2a-2**, **2b-1**, and **2b-2** were obtained by a Heck reaction between **1a-1**, **1a-2**, **1b-1**, **1b-2** and *p*-(methylthio)styryl. The 5-N position was methylated by iodomethane to obtain **3a-1, 3a-2, 3b-1** and **3b-2.** Then 11-position chlorine was substituted by different amino side chains to get the final **series I** and **series II** products.

Binding Affinities and Selectivity of MSQ Derivatives on NRAS RNA G-Quadruplex. Surface plasmon resonance (SPR) experiments were firstly performed for investigating the binding affinities of the derivatives with the *NRAS* RNA G-quadruplex nucleotide (NRQ, **Supplementary Table S1**), as well as their binding affinity for mutant *NRAS* RNA (NRQ-mutant, **Supplementary Table S1**) and the hairpin DNA. A previous synthesized quindoline derivative, compound **16**, was used as a control (**Supplementary Figure S1**). The dissociation constants (K_D) were determined by the equilibrium fitting mode (**Supplementary Figure S2**) and listed in **Table 1**. The data showed that several **MSQ** derivatives bound to the NRQ with high affinities, which were similar to that of the reference compound **16**. We collected all the compounds showing binding abilities to the NRQ and made a histogram in **Figure 2**. Compound **4a-10** and **4a-16** showed strongest binding affinities with the NRQ (**Figure 5a** and **5b**), with K_D values of 0.7 ± 0.1 μmol/L (**4a-10**), and 0.5 ± 0.2 μmol/L (**4a-16**), respectively. On the other hand, we noticed that the methylation at the

5-position made these compounds strongly bind to all the tested oligomers, just like the reference compound **16**.

Table 1. K_D values (μmol/L) of **MSQ** compounds with NRQ, NRQ-mutant, and hairpin oligomers in SPR experiments using an equilibrate fitting model.

	NRQ	NRQ-mutant	hairpin		NRQ	NRQ-mutant	hairpin
4a-1	14.9±2.3	N.A.[a]	N.A.	**4a-24**	N.A.	N.A.	N.A.
4a-2	17.2±5.4	N.A.	N.A.	**4a-25**	N.A.	N.A.	N.A.
4a-3	6.4±0.7	N.A.	N.A.	**4a-26**	3.4±0.3	N.A.	N.A.
4a-4	14.4±3.5	N.A.	N.A.	**4b-1**	1.3±0.3	N.A.	N.A.
4a-5	5.7±0.5	N.A.	N.A.	**4b-2**	N.A.	N.A.	N.A.
4a-6	N.A.	N.A.	N.A.	**4c-1**	15.8±2.8	N.A.	N.A.
4a-7	N.A.	N.A.	N.A.	**4c-2**	3.1±0.2	37.2±24.9	14.1±3.2
4a-8	N.A.	N.A.	N.A.	**4c-3**	21.2±13.0	N.A.	N.A.
4a-9	4.8±1.5	N.A.	N.A.	**4c-4**	4.1±1.2	N.A.	N.A.
4a-10	0.7±0.1	N.A.	N.A.	**4c-5**	1.7±0.8	N.A.	N.A.
4a-11	4.5±0.2	N.A.	N.A.	**4c-6**	N.A.	N.A.	N.A.
4a-12	N.A.	N.A.	N.A.	**4d-1**	10.4±2.0	2.74E-05	9.13E-06
4a-13	N.A.	N.A.	N.A.	**4d-2**	5.9±2.5	N.A.	N.A.
4a-14	N.A.	N.A.	N.A.	**5a-10**	3.4±1.7	4.8±2.4	2.2±1.1
4a-15	N.A.	N.A.	N.A.	**5a-16**	1.4±0.6	3.1±1.6	10.4±6.5
4a-16	0.5±0.2	N.A.	N.A.	**5b-1**	1.2±0.2	1.9±10	2.7±0.9
4a-17	2.3±0.4	N.A.	N.A.	**5b-2**	0.8±0.1	2.2±1.4	2.7±0.9
4a-18	N.A.	N.A.	N.A.	**5c-5**	2.9±1.5	3.2±2.0	2.0±1.0
4a-19	2.6±0.2	N.A.	N.A.	**5c-6**	1.2±0.5	1.3±1.2	1.0±0.8
4a-20	1.0±0.3	N.A.	N.A.	**5d-1**	1.3±0.4	2.0±0.1	5.3±2.4
4a-21	N.A.	N.A.	N.A.	**5d-2**	2.6±0.6	1.3±0.2	6.9±3.3
4a-22	N.A.	N.A.	N.A.	**16**	1.0±0.1	9.5±1.6	3.1±0.3
4a-23	N.A.	N.A.	N.A.				

[a] N.A. indicates not available between compounds and the oligomers.

These results suggested that the introduction of the *p*-(methylthio)styryl could

benefit the binding affinity and selectivity with the NRQ. We analyzed the relationship between structures and activities. A common finding was that the side chains containing heterocyclic nitrogen facilitated the binding of these **MSQ** derivatives with the NRQ. While introduction of side chains containing amino ends didn't contribute to the binding with RNA G-quadruplex, which was inconsistent with the previous findings in DNA G-quadruplex.[24] Besides, comparing the data in compounds **4a-4** and **4a-10**, we could find that longer side chains seemed to facilitate the binding.

The side chain of **4a-10** was N-methyl-2-(pyrrolidin-1-yl)ethan-1-amine, we further analyzed other derivatives containing the same side chain (**4a-10**, **5a-10**, **4b-2**, **4c-6**, **4d-2**, **5b-2**, **5c-6**, and **5d-2**). **5a-10** and **4a-10** possess similar structure, the only difference is the 5-position of **5a-10** was methylated. **5a-10** has similar binding affinity with **4a-10** but poor selectivity, which was also observed in other 5-methylated derivatives (**5c-6**, **5b-2** and **5d-2**). The *p*-(methylthio)styryl of **4b-2** and **4d-2** were at the 3-position, which caused an obvious decrease in the binding affinity. As for **4c-6**, which is a 10H-indolo[*3,2-b*]quinoline derivative instead of a benzofuro[3,2-b]quinoline derivative, could not bind to RNA G-quadruplex anymore. This is also inconsistent with the findings in DNA G-quadruplex's ligands.[24]

Effects of MSQ Derivatives on Proliferation of Tumor Cells. In order to investigate the cell proliferation inhibitory activities of **MSQ** derivatives on different cancer cell lines, a methyl thiazolyl tetrazolium (MTT) colorimetric assay was

performed. Here we used a human normal colon mucosal epithelial cell line NCM460 and six human tumor cell lines, including human melanoma cell line A375, human lung adenocarcinoma cell line A549, human cervical cancer cell line Hela, human hepatoma cell lines Huh7, human colon cancer cell line HCT116, and human breast cancer cell line MCF-7. Comparing to another cell line (such as human bone osteosarcoma epithelial cells U2OS), NRAS overexpresses in the selected six cancer cell lines (**Supplementary Figure S3**). The concentration for 50% inhibition (IC_{50}) values of all the derivatives were listed in **Supplementary Table S2** and **Figure 3**. As the results showed, most of the compounds had strong inhibitory activities on these tumor cells proliferation, with the IC_{50} varying from 0.5 μM to 10 μM. Compounds **4a-4**, **4a-6~4a-8**, **4a-12**, **4a-13**, **4a-18**, **4a-22**, and **4a-25** could not show any effects on cells proliferation at the highest tested concentration 50 μM. Comparing the data obtained in the SPR experiment, these compounds could not bind to the NRQ except **4a-4** had weak binding affinity. This indicated a consistent structure-activity relationship (SAR) with that in the SPR experiment.

We also compare the activities of **MSQ** compounds on the proliferation of normal cell line NCM460. **MSQ** compounds exhibited relatively weaker growth inhibition on NCM460 cells but the differences were not significant.

We further plotted the IC_{50} on A375 cells after exposure to each compound as a function of the binding between **MSQ** derivatives to the NRQ (**Figure 4a**) since A375 cells possesses high *NRAS* mutation rate.[43-45] Compounds falling into the lower left quadrant were those significantly bind to the NRQ; while compounds in the lower

right quadrant weakly bound to the NRQ, but still had effect on cell proliferation. Ligands of interest (shaded pink) appeared in the lower left quadrant, as these molecules possessing K_D values lower than 1 μM and IC_{50} less than 5 μM, including **4a-10**, **4a-16**, and **5b-2**. Considering the poor selectivity of **5b-2** on the NRQ *vs.* NRQ-mutant and hairpin, we selected **4a-10** and **4a-16** for further analysis and their structures were also shown in **Figure 4a**. We assessed the physiochemical properties of these two compounds using the 'Lipinski rule of five' criteria[46] (**Figure 4b**). The physiochemical properties of these two compounds actually were similar. Specifically, their molecular weight, polar surface area, number of hydrogen bond, and number of acceptors/donors fitted the 'Lipinski rule of five', but the hydrophobicity was too high (cLogP was more than 5). For obtaining a better description of the real lipophilicity of a compound which is not neutral in the biological environment, we further calculated the logD at physiological pH condition. The cLogD values were 4.51 (**4a-10**) and 4.57 (**4a-10**), which were less than 5. Basing on the above data, we used both **4a-10** and **4a-16** in the further *in vitro* and cellular assays.

Interactions of MSQ Derivatives with the *NRAS* RNA G-quadruplex. Circular dichroism (CD), ultraviolet visible (UV-vis), and fluorescence spectroscopy were used here to identify the interactions of **4a-10** and **4a-16** with the *NRAS* RNA G-quadruplex. Firstly, we incubated the compounds with the NRQ sequence and made them anneal to form the G-quadruplex structure in the absence or presence of potassium. CD spectroscopy was applied to identify the signal of these complex. As

the results showed in **Supplementary Figure S4a** and **S4b**, the NRQ exhibited a positive peak at around 262 nm and a negative peak at around 240 nm, which could be significantly increased by 100 mM potassium. This indicated the formation of the G-quadruplex structure in this oligomer. After the addition of compound **4a-10** and **4a-16**, the peak at 262 nm was more obvious in the potassium-lack complex and an induced CD (ICD) signal could be observed at around 350 nm.[47] Both the increased peak and the appearance of induced CD signal in the absence of potassium indicated **4a-10** and **4a-16** had interactions with the *NRAS* RNA G-quadruplex structure. However, the intensity of the ellipticity in the presence of potassium changed little after the addition of these compounds. This might due to a very stable G-quadruplex structure under this situation, and no conformational change by the compounds. Besides, the reduction of the ICD signal under this situation might come from the change of binding sites between compounds and the G-quadruplex structures in different conditions.[47]

Then, titration experiments were performed by using both UV-vis and fluorescence spectroscopy. In the UV-vis titration experiments, the concentrations of **4a-10** and **4a-16** were kept at 5 μmol/L, and the NRQ oligomer was titrated into the solution. As shown in **Figure 5c** and **5d**, there exhibited a distinct hypochromic effect at both two peaks (340 nm and 428 nm) and a weak blue shift along with the titration of the NRQ oligomer, which indicated a strong π-π interaction between the aromatic planar of compounds and the terminal G-quartets of the *NRAS* RNA quadruplex. In addition, by using a sigmoidal (Hill model) fitting (the insets in **Figure 5c** and **5d**),

K_D values were calculated as 1.47 ± 0.1 μmol/L (**4a-10**) and 1.98 ± 0.4 μmol/L (**4a-16**).

Furthermore, the fluorescent titration and Job's plot measurements were also applied to obtain more binding information. As showed in **Supplementary Figure S5a** and **S5b,** both the compounds exhibited a maximum emission at 542 nm upon an excitation at 430 nm. Contrary to the results in the UV titration, the fluorescent intensity increased upon the increasing of NRQ. By using the sigmoidal fitting (**Supplementary Figure S5c** and **S5d**), the K_D values were calculated as 2.50 ± 0.95 μmol/L (**4a-10**) and 0.75 ± 0.16 μmol/L (**4a-16**). These K_D values were similar with those in the UV titration assays. On the other hand, Job's plot analysis was also applied to determine the stoichiometry between the RNA and the compounds. The fitting curve suggested the formation of a 2:1 complex with two **4a-10** for one G-quadruplex, while a 1:1 complex with one **4a-16** for one G-quadruplex (**Supplementary Figure S5e** and **S5f**). The different stoichiometry of **4a-10** and **4a-16** might be due to their different binding sites, which still needs more supportive evidence (study is undergoing and data is not shown in this manuscript).

On the other hand, an important index for G-quadruplex ligands is the changes in melting temperature (ΔT_m) of quadruplex-forming oligomers, which indicates the effects on the thermostability of the nucleic acids. We investigated the melting temperatures (T_m) of the NRQ oligomer in the absence or presence of the compounds by using the CD spectroscopy. The spectrogram at each tested temperatures and the fitted melting curves were shown in **Figure 6**. In the absence of compounds, the T_m

value of the NRQ oligomer was 49.2 ± 0.5 ^{o}C, and both **4a-10** and **4a-16** increased the T_m value to 66.7 ± 0.3 ^{o}C and 57.1 ± 0.2 ^{o}C, respectively. Since we aimed to find a novel RNA G-quadruplex ligand, we further identified the effect of **4a-10** on the thermostabilities of DNA G-quadruplexes, including TBA, RET, and HTG21 (**Supplementary Table S1**). As shown in **Supplementary Figure S6**, after the addition of **4a-10**, T_m values of all three oligomers could not show a significant change.

Together with the data from CD spectroscopy, UV and fluorescence titration, **4a-10** and **4a-16** could bind to the NRQ oligomer and stabilize this oligomer. The binding stoichiometry of the two compounds might be a slightly different and **4a-10** showed a stronger ability on stabilization than **4a-16**.

Repression of *NRAS*'s Translation by the Compounds. Before all the further cellular experiments, we noticed that the differences of **MSQ** compounds' inhibitory activities on normal cells and cancer cells actually were not obvious in the MTT assay (**Figure 3**). Thus, we evaluated the effect of the strongest compound **4a-10** on cells proliferation by using the real-time cellular analysis (RTCA). As shown in **Supplementary Figure S7**, **4a-10** could inhibit A375 cells' proliferation at low concentrations in 72-hour treatment. However, the situation in primary cultured mouse mesangial cells was complicated. After the addition of **4a-10**, these primary cells quickly showed an inhibition on proliferation but then an increase on proliferation after 36-hour of treatment. At the end of experiment (72 h), the cell

index in **4a-10**-treated groups were even higher than that in the control group, which indicated that this compound might not inhibit the normal cells' proliferation.

The RNA G-quadruplex plays as a translational repressor for the *NRAS* gene.[12] Therefore, we investigated the regulation of **4a-10** and **4a-16** on the translation of the *NRAS* gene in A375 cells by using Western blot assays. As shown in **Figure 7**, **4a-10** could repress the translation of *NRAS* while **4a-16** somehow could increase the translation. In fact, this was unexpected thus we further verified it in MCF-7, Hela, and A549 cells. As shown in **Supplementary Figure S8**, **4a-10** could also repress the expression of NRAS in all these cells while **4a-16** could not show effect or even a little simulative effect on NRAS's expression. From the above data in Job's plot (**Supplementary Figure S5**), we found the different stoichiometry of **4a-10** and **4a-16** thereby different binding sites. The diverse effects of these two compounds on NRAS's translation might also an imply of this hypothesis because different binding sites might cause different interfering effects on proteins' recognition and binding to the RNA. Anyway, since we aimed to find out a novel *NRAS* translational repressor here, we decided to use only **4a-10** in our further cellular assays. The study on detailed effect and mechanism of **4a-16** on *NRAS*'s translation is still in progress which is not shown in this manuscript anymore.

Moreover, the effect of **4a-10** on *NRAS*'s transcription and translation was further identified by using quantitative real time polymerase chain reaction (qRT-PCR) (**Figure 8a** and **8b, Supplementary Figure S9**), Western blot (**Figure 7** and **8c**), dual-luciferase (**Figure 8d** and **8e**), and RNA immunoprecipitation (RIP) assays

(**Figure 8f**). The results in qRT-PCR and Western blot indicated that **4a-10** could inhibit the expression of *NRAS* at a concentration of 0.02 μmol/L, but had no effect on the transcription of *NRAS* from 0.02 to 0.5 μmol/L. To be noted, dual-luciferase assay could not be done in A375 cells due to extremely low response values in these cells and we used MCF-7 here. In order to be consistent with the dual luciferase experiment, the repression effects on NRAS's expression was also confirmed in MCF-7 cells (**Figure 8c**). Dual-luciferase reporter assay was then performed using a psicheck2 plasmid carrying the *NRAS* 5'-UTR wild-type or mutant clones (**Supplementary Table S1**) in front of the Renilla luciferase. The same plasmid carrying Firefly luciferase was used as an internal control. After transfection these plasmids into MCF-7 cells for 6 h, **4a-10** at increasing concentrations was added into cells and incubated for another 48 h. The ratio of *Renilla/Firefly* luciferase within the plasmid containing the wild-type *NRAS* 5'-UTR decreased to 63.6% at the concentration of 0.5 μM (**Figure 8d**). In contrast, in the mutant group (**Figure 8e**), the results did not change significantly with the increase in concentration. These results indicated **4a-10** might repress the translation of the *NRAS* gene by binding to the RNA G-quadruplex in the 5'-UTR of *NRAS*.

In general, the switch of G-quadruplex structures and other secondary structures in the regulation region will influence on the recognition and binding of transcriptional factors or translational factors.[48] For example, nucleic acids unwinding proteins such as Werner syndrome protein (WRN)[16], Bloom protein (BLM)[49], Fanconi anemia-associated DNA helicase (FANCJ)[50], DEAH (Asp-Glu-Ala-His) box RNA

helicase 36 (DHX36)[51], or PIF1[52], can unfold G-quadruplex structures. Among them, the DHX36 RNA helicase binds specifically to the parallel-stranded G-quadruplexes in RNAs and resolves them thereby regulating several mRNA-related processes.[53-58] Therefore, we further estimated whether the binding of DHX36 protein to the *NRAS* mRNA could be interfered by **4a-10** by using a RIP assay. After incubating the A375 cells with 2 μmol/L **4a-10**, complexes of the DHX36 antibody with its RNA targets were obtained using protein A/G plus agarose beads. The complexes were detected via RT-PCR (**Figure 8f**). The amount of DHX36-bound *NRAS* sequences reduced by **4a-10**, which indicated that the stabilization of the *NRAS* RNA G-quadruplex by **4a-10** could interfere with the binding and resolving of the DHX36 protein. This might be the major reason for **4a-10** to cause translational repression.

Cell Cycle Arrest at G_0/G_1 Phase by 4a-10. Since NRAS protein could participate in the process of cell cycle, we then carried out the flow cytometric assay to evaluate whether **4a-10** could regulate the cell cycle of A375 cells. After treated A375 cells with different concentration of **4a-10** for 24 h, the proportion of cells in each phase (G_0/G_1, S and G_2/M) was calculated by flow cytometric. As the results in **Figure 9a** and **9b**, the proportion of cells in the G_0/G_1 phase increased while the proportion of the G_2/M phase decreased after the treatment of **4a-10**. In other word, **4a-10** could arrest A375 cells in the G_0/G_1 phase in a dose-dependent manner, with a maximum increase of 13% at the highest concentration of 0.5 μM.

In addition, we concerned whether **4a-10** could effectively be absorbed into the

cells. Therefore, we performed cellular uptake experiment, and found about 65% of **4a-10** could be uptaken into A375 cells after 6-hour treatment (**Supplementary Figure S10**). Besides, as the strong fluorescent character of **4a-10**, we used confocal microscopy to determine the cellular internalization of **4a-10**. A375 cells were treated with 1.0 μM **4a-10** for 6 h, then cells were fixed and dyed with the nucleus dye 4',6-diamidino-2-phenylindole (DAPI). As shown in **Figure 9c**, **4a-10** mainly localized in the cytoplasm. This further supported the credibility of the above cellular experiments.

■ CONCLUSIONS

In the present study, we designed and synthesized novel **MSQ** derivatives combined the 4-(methylthio) styryl moiety from the RNA-specific chemical probes, with the quindoline scaffold for specifically targeting to the *NRAS* RNA G-quadruplex. 44 novel compounds were synthesized and the binding activities to the RNA G-quadruplex and inhibitory activities on tumor cells proliferation were evaluated. Structure-activity relationships (SAR) analysis suggested that the *p*-(methylthio)styryl side chains, especially those introduced at the 2-position, could greatly enhanced the binding affinities and selectivity to the RNA G-quadruplex. On the other hand, the 5-N-positon methylation could improve the G-quadruplex binding affinity with poor binding selectivity. According to these data together with other *in vitro* data, we chose **4a-10** as the hit to further evaluate its effect on human melanoma cells A375. All the *in vitro* and cellular results indicated that **4a-10** could bind and stabilize the RNA

G-quadruplex in *NRAS*'s 5'-UTR region, and thus repressed NRAS's translation and arrested the cells at G_0/G_1 phase. We noticed that **4a-10** and **4a-16**, who possessed similar binding constants with the NRQ oligomer and similar stabilizing activities, showed diverse effects on NRAS's translation. This behavior was unexpected and seemed to go against our hypothesis. Actually, the different stoichiometry of **4a-10** and **4a-16** might be due to their different binding sites. The diverse effects of these two compounds on NRAS's translation might also come from the different binding sites since different binding sites might cause different interfering effects on proteins' recognition and binding to the RNA. We are trying to figure out the reason and thorough studies are still undergoing (data not shown).

From the present study, we found that the experience in DNA G-quadruplex ligands design might not be 100% suitable for that in RNA. This is interesting but still needs more data from structural modification and SAR analysis to confirm. And of course, accurate and thorough mechanic studies will benefit to concluding the real modification rule.

Taken together, we herein provided a novel strategy for developing RNA G-quadruplex ligands from the typical DNA G-quadruplex ligands, which is helpful for discovery novel RNA G-quadruplex ligands as anti-cancer drugs.

■ EXPERIMENTAL SECTION

General Methods in Synthesis. All chemicals were purchased from commercial sources unless otherwise specified. All chemical structures were

confirmed by ^{1}H and ^{13}C nuclear magnetic resonance (NMR) spectra and high-resolution mass spectrometer (HRMS). ^{1}H and ^{13}C NMR spectra were recorded using tetramethylsilane (TMS) as the internal standard in DMSO-d_6, CD_3OD or CDCl3 with a Bruker BioSpin GmbH spectrometer at 400 MHz and 100 MHz, respectively. HRMS were obtained with a MAT95XP (Thermo) mass spectrometer. Melting points (mp) were determined using an SRS-OptiMelt automated melting point instrument without correction. The purity of the synthesized compound was confirmed to be higher than 95% by using analytical high-performance liquid chromatography (HPLC) performed with a dual pump Shimadzu LC-20 AB system equipped with an Ultimate XB-C18 column (4.6 × 250 mm, 5 μm) and eluted with methanol-water (35:65-80:20) containing 0.1% trifluoroacetic acid (TFA) at a flow rate of 0.5 mL/min or 0.2 mL/min.

Synthesis of Intermediates 2a-1, 2a-2, 2b-1, and 2b-2. The intermediate **1a-1**, **1a-2**, **1b-1**, and **1b-2** were prepared following the procedures previously reported.[40] Then, 750 mg of compounds **1a-1, 1a-2, 1b-1**, or **1b-2**, 55 mg of palladium(II) acetate (0.24 mmol), 230 mg of tri-ortho-tolylphosphine (0.76 mmol), 1.25 mL *p*-(methylthio)styryl (8.3 mmol), and 7 mL anhydrous triethylamine were added to 21-mL anhydrous tetrahydrofuran under argon atmosphere at 0 ^{o}C. The solution was stirred at 110 ^{o}C for 40 h. The mixture was then cooled to room temperature, poured into ice water (200 mL) and extracted with dichloromethane (100 mL × 3). Then organic layer was collected and washed with water, brine and dried over anhydrous sodium sulfate. After removing dichloromethane at a reduced pressure,

crude product was purified by column chromatography on silica gel with CH_2Cl_2/MeOH (500:1) as eluent to obtain yellow solid in 59% ~ 70% yield.

General Method for the Synthesis of Intermediates 3a-1, 3a-2, 3b-1 and 3b-2. 200 mg of compounds **2a-1, 2a-2, 2b-1** or **2b-2**, and 2 g of iodomethane (14.09 mmol) were added to 1-mL tetramethylene sulfone. The mixture was stirred at 68 ^{o}C for 48 h. Then cooled to room temperature. 20 mL ether was added to precipitate the dark red solid. Solid was filtrated and washed with ether for three times and dried by vacuum to obtain red to dark red solid. Yield 75%~80%; Crude products used in next step directly.

General Method for the Synthesis of Compounds in Series I. 100 mg of compounds **2a-1, 2a-2, 2b-1**, or **2b-2**, 95 mg of *p*-toluenesulfonic acid monohydrate (0.5 mmol) were put in a dry sealed tube, then 1 mL amino side chain was added. The mixture was stirred at 120 ^{o}C for 16~24 h and the reaction was monitored intermittently by thin-layer chromatography (TLC). Then the mixture was cooled to room temperature. Ice water (20 mL) was poured into the mixture and extracted by trichloromethane (30 mL × 3). Then organic layer was collected and washed with water, brined and dried over anhydrous sodium sulfate. After removing trichloromethane at a reduced pressure, crude product was purified by column chromatography on silica gel with CH_2Cl_2/MeOH/Et_3N (250:1:0.1-50:1:0.1) as eluent to obtain yellow solid, yield 50% ~ 70%.

General Method for the Synthesis of Final products series II. 100 mg of compounds **3a-1**, **3a-2**, **3b-1**, or **3b-2**, and 0.25 mL amino side chain were added to

1-mL 2-ethoxyethanol. The mixture was stirred at 120 ^{o}C for 24 h. Then the solution was cooled to room temperature. 20 mL ether was added to precipitate, and then filtered, washed with ether for three times. Purified by recrystallization from MeOH/ hexane to get orange red to dark red solid, yield 75% ~ 80%.

(E)-11-chloro-2-(p-(methylthio)styryl)benzofuro[3,2-b]quinoline (2a-1). Yield 62%. ^{1}H NMR (400 MHz, $CDCl_3$) δ 8.34 (d, J = 7.7 Hz, 1H), 8.29 – 8.21 (m, 2H), 7.99 (dd, J = 9.0, 1.5 Hz, 1H), 7.67 (d, J = 3.0 Hz, 2H), 7.50 (d, J = 8.3 Hz, 3H), 7.29 (d, J = 1.7 Hz, 2H), 7.26 (d, J = 3.1 Hz, 2H), 2.54 (s, 3H). ^{13}C NMR (101 MHz, $CDCl_3$) δ 159.25, 146.64, 146.35, 144.72, 138.67, 136.02, 133.78, 131.13, 130.08, 129.89, 127.10, 126.61, 126.19, 125.62, 124.12, 123.07, 122.34, 121.52, 120.70, 112.40, 15.69. HRMS (ESI) m/z: calcd for $C_{24}H_{16}NOSCl$, $[M+H]^+$, 402.0714, found 402.0741.

(E)-11-chloro-2-(p-(methylthio)styryl)-10H-indolo[3,2-b]quinoline (2a-2). Yield 59%. ^{1}H NMR (500 MHz, DMSO) δ 11.83 (s, 1H), 8.36 – 8.30 (m, 2H), 8.24 (d, J = 8.9 Hz, 1H), 8.14 (d, J = 9.0 Hz, 1H), 7.71 – 7.57 (m, 5H), 7.48 (d, J = 16.4 Hz, 1H), 7.37 – 7.27 (m, 3H), 2.52 (s, 3H). ^{13}C NMR (126 MHz, DMSO) δ 145.99, 144.52, 144.06, 138.53, 135.73, 134.13, 130.92, 130.73, 130.21, 130.00, 127.86, 127.72, 126.51, 124.77, 124.52, 122.06, 121.82, 121.14, 120.79, 118.35, 112.53, 15.05. HRMS (ESI) m/z: calcd for $C_{24}H_{16}N_2SCl$, $[M+H]^+$, 401.0874, found 401.0860.

(E)-11-chloro-3-(p-(methylthio)styryl)benzofuro[3,2-b]quinoline (2b-1). Yield 70%. ^{1}H NMR (400 MHz, CDCl3) δ 8.30 (d, J = 7.7 Hz, 1H), 8.23 (dd, J = 5.1, 3.6 Hz, 2H), 7.83 (dd, J = 8.9, 1.5 Hz, 1H), 7.61 (d, J = 3.6 Hz, 2H), 7.44 (d, J = 8.2

Hz, 3H), 7.22 (d, J = 2.5 Hz, 2H), 7.19 (d, J = 3.8 Hz, 2H), 2.46 (s, 3H). ^{13}C NMR (101 MHz, $CDCl_3$) δ 158.36, 146.60, 146.17, 137.69, 136.88, 134.22, 132.81, 130.31, 129.30, 126.16, 126.01, 125.67, 123.98, 123.70, 123.15, 122.77, 122.02, 121.49, 120.14, 111.48, 14.72. HRMS (ESI) *m/z*: calcd for $C_{24}H_{16}NOSCl$, $[M+H]^+$, 402.0721, found 402.0714.

(E)-11-chloro-3-(p-(methylthio)styryl)-10H-indolo[3,2-b]quinoline(2b-2). Yield 70%. ^{1}H NMR (500 MHz, DMSO) δ 11.85 (s, 1H), 8.36 (d, J = 7.9 Hz, 2H), 8.25 (d, J = 8.8 Hz, 1H), 8.07 (d, J = 8.9 Hz, 1H), 7.72 – 7.60 (m, 4H), 7.50 (s, 2H), 7.35 (t, J = 7.4 Hz, 1H), 7.31 (d, J = 8.2 Hz, 2H), 2.52 (s, 3H). ^{13}C NMR (126 MHz, DMSO) δ 146.84, 144.80, 144.54, 138.43, 136.35, 134.13, 130.82, 130.45, 129.66, 127.73, 127.64, 126.51, 124.61, 123.57, 122.98, 122.17, 121.70, 120.76, 118.63, 112.58, 15.07. HRMS (ESI) m/z: calcd for $C_{24}H_{16}N_2SCl$, $[M+H]^+$, 401.0874, found 401.0865.

(E)-N^1,N^1-dimethyl-N^2-(2-(p-(methylthio)styryl)benzofuro[3,-2b]quin-olin-1 1-yl) ethane-1,2-diamine (4a-1). Compounds **2a-1** was reacted with 2-dimethylaminoethylamine according to general procedure to afford **4a-1** as a yellow solid. Yield 67%. ^{1}H NMR (400 MHz, CDCl3) δ 8.32 (d, J = 7.6 Hz, 1H), 8.11 (d, J = 8.9 Hz, 1H), 7.90 (dd, J = 8.9, 1.3 Hz, 1H), 7.79 (s, 1H), 7.53 (dt, J = 12.2, 7.5 Hz, 2H), 7.46 (d, J = 8.3 Hz, 2H), 7.39 (dd, J = 10.6, 3.8 Hz, 1H), 7.27 – 7.20 (m, 3H), 7.14 (d, J = 16.3 Hz, 1H), 5.90 (s, 1H), 4.11 (dd, J = 11.0, 5.3 Hz, 2H), 2.75 (t, J = 5.8 Hz, 2H), 2.50 (s, 3H), 2.37 (d, J = 18.0 Hz, 6H). ^{13}C NMR (101 MHz, $CDCl_3$) δ 158.15, 146.91, 146.84, 137.96, 134.57, 134.37, 134.30, 132.73, 130.05, 129.73,

128.22, 127.95, 126.92, 126.72, 125.00, 123.68, 123.01, 121.95, 119.53, 118.32, 111.83, 58.61, 45.32, 42.53, 15.82. HRMS (ESI) m/z: calcd for C_{28} H_{27} N_3OS, $[M+H]^+$. 454.1948, found 454.1958. HPLC purity: 98.7%.

(E)-N^1,N^1-diethyl-N^2-(2-(p-(methylthio)styryl)benzofuro[3,2-b]quinol-in-11-yl) ethane-1,2-diamine (4a-2). Compounds **2a-1** was reacted with N,N-diethylethylenediamine according to general procedure to afford **4a-2** as a yellow solid. Yield 70 %. ^{1}H NMR (400 MHz, $CDCl_3$) δ 7.79 (d, J = 7.6 Hz, 1H), 7.56 (d, J = 8.8 Hz, 1H), 7.29 (dd, J = 13.4, 9.6 Hz, 3H), 7.04 – 6.95 (m, 2H), 6.92 – 6.83 (m, 3H), 6.72 (d, J = 1.5 Hz, 1H), 6.63 (d, J = 2.5 Hz, 2H), 3.68 (dd, J = 10.0, 5.1 Hz, 2H), 2.17 – 2.05 (m, 2H), 1.97 (s, 3H), 1.91 (s, 6H), 1.48 – 1.42 (m, 2H).; ^{13}C NMR (101 MHz, $CDCl_3$) δ 158.16, 146.91, 146.82, 137.98, 134.69, 134.36, 134.30, 132.70, 129.97, 129.72, 128.19, 127.94, 126.90, 126.74, 125.49, 123.71, 123.00, 121.98, 119.13, 118.47, 111.83, 52.30, 46.81, 42.37, 15.83, 12.27. HRMS (ESI) *m/z*: calcd for C_{29} $H_{29}N_3OS$, $[M+H]^+$, 468.2104, found 468.2106. HPLC purity: 99.5%.

(E)-N^1,N^1-dimethyl-N^3-(2-(p-(methylthio)styryl)benzofuro[3,2-b]quin-olin-1 1-yl) propane-1,3-diamine (4a-3). Compounds **2a-1** was reacted with 3-dimethylaminopropylamine according to general procedure to afford **4a-3** as a yellow solid. Yield 70%. ^{1}H NMR (400 MHz, $CDCl_3$) δ 8.20 (d, J = 7.7 Hz, 1H), 7.99 (d, J = 9.1 Hz, 1H), 7.80 – 7.72 (m, 2H), 7.43 (dt, J = 10.0, 8.4 Hz, 2H), 7.36 (d, J = 8.3 Hz, 2H), 7.28 (t, J = 7.9 Hz, 1H), 7.15 (d, J = 8.4 Hz, 2H), 7.11 – 7.06 (m, 2H), 6.07 (s, 1H), 3.98 (dd, J = 10.8, 5.2 Hz, 2H), 2.80 (t, J = 5.8 Hz, 2H), 2.59 (dd, J = 14.1, 7.1 Hz, 4H), 2.39 (s, 3H), 1.04 (t, J = 7.1 Hz, 6H). ^{13}C NMR (101 MHz, $CDCl_3$)

δ 158.16, 146.91, 146.82, 137.98, 134.69, 134.36, 134.30, 132.70, 129.97, 129.72, 128.19, 127.94, 126.90, 126.74, 125.49, 123.71, 123.00, 121.98, 119.13, 118.47, 111.83, 52.30, 46.81, 42.37, 15.83, 12.27. HRMS (ESI) *m/z*: calcd for $C_{30}H_{31}N_3OS$, $[M+H]^+$, 482.2261, found 482.2266. HPLC purity: 97.7%.

(E)-11-(4-methylpiperazin-1-yl)-2-(p-(methylthio)styryl)benzofuro[3,2-b] quinoline (4a-4). Compounds **2a-1** was reacted with 1-methylpiperazine according to general procedure to afford **4a-4** as a yellow-green solid. Yield 68 %. ^{1}H NMR (400 MHz, $CDCl_3$) δ 8.33 (d, J = 7.5 Hz, 1H), 8.18 (d, J = 8.8 Hz, 2H), 7.93 (d, J = 9.1 Hz, 1H), 7.58 (dd, J = 20.0, 8.0 Hz, 2H), 7.50 (d, J = 8.3 Hz, 2H), 7.42 (t, J = 7.2 Hz, 1H), 7.33 – 7.25 (m, 3H), 7.19 (d, J = 16.3 Hz, 1H), 3.80 – 3.64 (m, 4H), 2.79 (s, 4H), 2.51 (s, 3H), 2.48 (s, 3H); ^{13}C NMR (101 MHz, $CDCl_3$) δ 160.79, 158.65, 147.68, 147.44, 141.56, 138.17, 137.59, 134.17, 133.85, 130.44, 129.89, 128.78, 128.07, 127.01, 126.68, 125.19, 124.08, 123.42, 123.13, 122.86, 122.10, 112.08, 55.73, 52.02, 46.45, 15.78. HRMS (ESI) *m/z*: calcd for $C_{30}H_{31}N_3OS$, $[M+H]^+$, 466.1948, found 466.1935. HPLC purity: 96.9%.

(E)-2-(p-(methylthio)styryl)-N-(2-(piperidin-1-yl)ethyl)benzofuro[3,2-b]quinolin-11-amine (4a-5). Compounds **2a-1** was reacted with 2-piperidin-1-ylethanamine according to general procedure to afford **4a-5** as a yellow solid. Yield 72 %. ^{1}H NMR (400 MHz, CDCl3) δ 8.36 (d, J = 7.5 Hz, 1H), 8.15 (d, J = 8.8 Hz, 1H), 7.97 (s, 1H), 7.91 (dd, J = 8.9, 1.7 Hz, 1H), 7.58 (dt, J = 11.2, 4.5 Hz, 2H), 7.51 (d, J = 8.4 Hz, 2H), 7.46 – 7.41 (m, 1H), 7.30 (d, J = 8.4 Hz, 2H), 7.24 (t, J = 10.7 Hz, 2H), 6.35 (s, 1H), 4.16 (dd, J = 11.1, 5.3 Hz, 2H), 2.85 (t, J = 5.9 Hz, 2H), 2.61 (d, J = 8.4 Hz, 4H),

2.55 (s, 3H), 1.75 (dt, J = 10.9, 5.6 Hz, 4H), 1.59 (d, J = 5.2 Hz, 2H); ^{13}C NMR (101 MHz, $CDCl_3$) δ 158.16, 146.83, 146.77, 137.98, 134.74, 134.42, 134.28, 132.68, 129.88, 129.71, 128.11, 127.89, 126.86, 126.71, 125.68, 123.65, 122.99, 121.98, 118.91, 118.48, 111.84, 57.54, 54.18, 41.59, 26.49, 24.49, 15.80. HRMS (ESI) *m/z*: calcd for $C_{31}H_{31}N_3OS$, $[M+H]^+$, 494.2265, found 494.2261. HPLC purity: 98.9%.

(E)-N-(4-fluorophenethyl)-2-(p-(methylthio)styryl)benzofuro[3,2-b]q-uinolin -11-amine (4a-6). Compounds **2a-1** was reacted with 4-fluorophenethylamine according to general procedure to afford **4a-6** as a yellow solid. Yield 60%. ^{1}H NMR (400 MHz, DMSO) δ 8.48 (s, 1H), 8.19 (d, J = 7.6 Hz, 1H), 7.96 (s, 2H), 7.77 (d, J = 8.2 Hz, 1H), 7.69 (t, J = 7.6 Hz, 1H), 7.59 (d, J = 8.1 Hz, 2H), 7.54 – 7.44 (m, 2H), 7.43 – 7.29 (m, 5H), 7.14 (t, J = 8.6 Hz, 2H), 4.13 (dd, J = 13.3, 6.6 Hz, 2H), 3.13 – 3.00 (m, 2H), 2.52 (s, 3H).^{13}C NMR (101 MHz, DMSO) δ 157.84, 147.00, 146.28, 138.15, 135.88, 135.84, 135.27, 134.30, 133.30, 132.68, 131.17, 131.09, 130.60, 129.82, 128.49, 128.07, 127.32, 126.66, 126.60, 123.80, 123.66, 121.91, 120.85, 118.65, 115.70, 115.49, 112.61, 46.89, 36.94, 15.09. HRMS (ESI) *m/z*: calcd for $C_{32}H_{25}N_2OFS$, $[M+H]^+$, 505.1744, found 505.1750. HPLC purity: 96.1%.

(E)-2-((2-(p-(methylthio)styryl)benzofuro[3,2-b]quinolin-11-yl)amino)-ethan -1-ol (4a-7). Compounds **2a-1** was reacted with ethanolamine according to general procedure to afford 4a-**7** as a yellow solid. Yield 65 %. ^{1}H NMR (400 MHz, DMSO) δ 8.65 (s, 1H), 8.26 (s, 1H), 7.99 (s, 2H), 7.77 (d, J = 7.9 Hz, 1H), 7.72 (d, J = 7.0 Hz, 1H), 7.59 (d, J = 8.1 Hz, 2H), 7.48 (dd, J = 16.8, 11.8 Hz, 2H), 7.33 (t, J = 12.7 Hz, 3H), 4.98 (s, 1H), 4.08 (d, J = 5.1 Hz, 2H), 3.81 (d, J = 4.7 Hz, 2H), 2.52 (s, 3H). ^{13}C

NMR (101 MHz, DMSO) δ 157.67, 138.23, 134.19, 133.06, 131.09, 128.83, 127.71, 127.50, 127.38, 126.60, 124.00, 122.24, 121.12, 118.23, 112.81, 99.99, 61.31, 47.84, 15.05. HRMS (ESI) *m/z*: calcd for $C_{26}H_{22}N_2O_2S$, $[M+H]^+$, 427.1475, found 427.1479. HPLC purity: 95.9%.

(E)-N-isobutyl-2-(p-(methylthio)styryl)benzofuro[3,2-b]quinolin-11a-mine (4a-8). Compounds **2a-1** was reacted with 2-methylpropanamine according to general procedure to afford **4a-8** as a yellow solid. Yield 68 %. ^{1}H NMR (400 MHz, DMSO) δ 8.56 (s, 1H), 8.19 (d, J = 7.3 Hz, 1H), 7.96 (s, 2H), 7.74 (d, J = 8.0 Hz, 1H), 7.70 – 7.63 (m, 1H), 7.59 (d, J = 7.7 Hz, 2H), 7.49 – 7.41 (m, 2H), 7.37 (d, J = 10.5 Hz, 2H), 7.31 (d, J = 7.7 Hz, 2H), 3.76 (s, 2H), 2.52 (s, 3H), 2.16 – 1.99 (m, 1H), 1.04 (d, J = 6.1 Hz, 6H); ^{13}C NMR (101MHz, DMSO) δ 157.72, 147.06, 146.24, 138.08, 135.74, 134.33, 133.26, 132.60, 130.48, 129.82, 128.36, 128.14, 127.30, 126.64, 126.38, 123.73, 123.67, 121.86, 121.09, 118.60, 112.58, 52.49, 30.09, 20.52, 15.08. HRMS (ESI) *m/z*: calcd for $C_{28}H_{26}N_2OS$, $[M+H]^+$, 439.1833, found 439.1839. HPLC purity: 98.4%.

(E)-2-(p-(methylthio)styryl)-N-(2-morpholinoethyl)benzofuro[3,2-b]-quinoli n-11-amine (4a-9). Compounds **2a-1** was reacted with 2-morpholin-4-ylethanamine according to general procedure to afford **4a-9** as a yellow solid. Yield 72 %. ^{1}H NMR (400 MHz, $CDCl_3$) δ 8.11 (d, J = 7.3 Hz, 1H), 7.90 (d, J = 8.8 Hz, 1H), 7.66 (d, J = 8.6 Hz, 1H), 7.61 (s, 1H), 7.39 – 7.26 (m, 2H), 7.24 (d, J = 7.8 Hz, 2H), 7.17 (t, J = 7.2 Hz, 1H), 7.03 (d, J = 8.0 Hz, 2H), 6.96 (t, J = 11.2 Hz, 2H), 5.79 (s, 1H), 3.91 (dd, J =10.2, 5.3 Hz, 2H), 3.59 (s, 4H), 2.62 (d, J = 5.3 Hz, 2H), 2.39 (s, 4H), 2.28 (s,

3H). ^{13}C NMR (101MHz, $CDCl_3$) δ 158.19, 146.77, 138.18, 134.45, 134.40, 134.12, 132.91, 130.04, 129.86, 128.43, 127.73, 126.90, 126.73, 125.51, 123.56, 123.11, 122.02, 118.79, 118.38, 111.84, 67.35, 57.48, 53.25, 41.28, 15.79. HRMS (ESI) *m/z*: calcd for $C_{30}H_{29}N_3O_2S$, $[M+H]^+$, 496.2053, found 496.2059. HPLC purity: 99.4%.

(E)-2-(p-(methylthio)styryl)-N-(2-(pyrrolidin-1-yl)ethyl)benzofuro-[3,2-b] quinolin-11-amine (4a-10). Compounds **2a-1** was reacted with 1-(2-aminoethyl)pyrrolidine according to general procedure to afford **4a-10** as a yellow solid. Yield 75 %. ^{1}H NMR (400 MHz, DMSO) δ 8.48 (s, 1H), 8.19 (d, J = 7.6 Hz, 1H), 7.95 (s, 2H), 7.75 – 7.63 (m, 2H), 7.58 (d, J = 8.1 Hz, 2H), 7.45 (dd, J = 15.9, 8.6 Hz, 1H), 7.39 – 7.33 (m, 2H), 7.31 (d, J = 7.8 Hz, 2H), 4.07 (dd, J = 13.2, 6.5 Hz, 2H), 2.83 (t, J = 6.9 Hz, 2H), 2.58 (d, J = 20.0 Hz, 4H), 2.52 (s, 3H), 1.71 (s, 4H). ^{13}C NMR (101 MHz, $CDCl_3$) δ 158.09, 146.71, 146.67, 137.90, 134.74, 134.26, 134.24, 132.68, 129.72, 128.10, 127.84, 126.89, 126.66, 125.28, 123.53, 123.01, 122.00, 119.39, 118.34, 111.82, 55.56, 53.95, 43.87, 23.68, 15.79. HRMS (ESI) *m/z*: calcd for $C_{30}H_{29}N_3OS$, $[M+H]^+$, 480.2104, found 480.2104. HPLC purity: 99.1%.

(E)-N-(3-(4-methylpiperazin-1-yl)propyl)-2-(p-(methylthio)styryl)-benzofuro [3,2-b]quinolin-11-amine (4a-11). Compounds **2a-1** was reacted with 1-(3-aminopropyl)-4-methylpiperazine according to general procedure to afford **4a-11** as a yellow solid. Yield 78 %. ^{1}H NMR (400 MHz, DMSO) δ 8.45 (s, 1H), 8.19 (d, J = 7.6 Hz, 1H), 7.96 (s, 2H), 7.73 – 7.63 (m, 2H), 7.58 (d, J = 8.3 Hz, 2H), 7.45 (dd, J = 14.6, 7.5 Hz, 1H), 7.40 – 7.26 (m, 5H), 4.00 (dd, J = 13.0, 6.6 Hz, 2H), 2.52 (s, 3H), 2.48 (d, J = 7.0 Hz, 2H), 2.34 (d, J = 43.3 Hz, 8H), 2.11 (s, 3H), 1.98 – 1.87 (m, 2H).

^{13}C NMR (101 MHz, $CDCl_3$) δ 158.02, 146.96, 146.82, 138.01, 135.26, 134.26, 134.18, 132.53, 130.02, 129.65, 128.34, 127.93, 126.90, 126.62, 124.84, 123.61, 122.94, 121.91, 120.35, 118.36, 111.81, 58.80, 55.28, 53.83, 46.80, 46.06, 25.69, 15.78. HRMS (ESI) *m/z*: calcd for $C_{32}H_{34}N_4OS$, $[M+H]^+$, 523.2526, found 523.2518. HPLC purity: 99.9%.

(E)-2-(p-(methylthio)styryl)-N-phenethylbenzofuro[3,2-b]quinolin-11-amine (4a-12). Compounds **2a-1** was reacted with 2-phenylethylamine according to general procedure to afford **4a-12** as a yellow solid. Yield 60 %. ^{1}H NMR (400 MHz, DMSO) δ 8.49 (s, 1H), 8.20 (d, J = 7.6 Hz, 1H), 8.02 – 7.92 (m, 2H), 7.77 (d, J = 8.2 Hz, 1H), 7.69 (t, J = 7.6 Hz, 1H), 7.59 (d, J = 8.0 Hz, 2H), 7.56 – 7.42 (m, 3H), 7.35 (dt, J = 15.2, 7.0 Hz, 7H), 7.23 (t, J = 7.0 Hz, 1H), 4.15 (dd, J = 13.9, 6.5 Hz, 2H), 3.16 – 3.02 (m, 2H), 2.52 (s, 3H). ^{13}C NMR (101 MHz, DMSO) δ 157.86, 147.03, 146.30, 139.72, 138.14, 135.29, 134.31, 133.31, 132.66, 130.60, 129.83, 129.36, 128.95, 128.47, 128.07, 127.32, 126.67, 126.61, 123.79, 123.70, 121.92, 120.85, 118.67, 112.58, 46.96, 37.89, 15.09. HRMS (ESI) *m/z*: calcd for $C_{32}H_{26}N_2OS$, $[M+H]^+$, 487.1839, found 487.1839. HPLC purity: 98.8%.

(E)-2-(p-(methylthio)styryl)-N-(2-(thiophen-2-yl)ethyl)benzofuro-[3,2-b] quinolin-11-amine (4a-13). Compounds **2a-1** was reacted with thiophene-2-ethylamine according to general procedure to afford **4a-13** as a yellow solid. Yield 58 %. ^{1}H NMR (400 MHz, $CDCl_3$) δ 8.18 (d, J = 7.6 Hz, 1H), 7.98 (d, J = 8.8 Hz, 1H), 7.74 (d, J = 8.8 Hz, 1H), 7.52 (s, 1H), 7.44 (d, J = 3.5 Hz, 2H), 7.31 (d, J = 8.1 Hz, 2H), 7.12 (s, 1H), 7.07 (d, J = 5.2 Hz, 1H), 7.00 (t, J = 12.1 Hz, 2H),

6.90 – 6.82 (m, 1H), 6.78 (s, 1H), 5.03 (s, 1H), 4.16 (dd, *J* = 13.0, 6.5 Hz, 2H), 3.20 (t, *J* = 6.6 Hz, 2H), 2.36 (s, 3H), 1.09 (s, 2H). ^{13}C NMR (101 MHz, $CDCl_3$) δ 158.23, 146.96, 146.78, 141.01, 138.11, 134.17, 134.09, 133.57, 133.02, 130.10, 129.95, 128.42, 127.68, 127.23, 126.90, 126.69, 125.84, 125.47, 124.34, 123.50, 123.20, 121.98, 118.68, 118.28, 111.96, 46.98, 31.66, 15.78. HRMS (ESI) *m/z*: calcd for $C_{30}H_{24}N_2OS_2$, $[M+H]^+$, 493.1403, found 493.1408. HPLC purity: 93.3%.

(E)-2-(p-(methylthio)styryl)-N-((tetrahydrofuran-2-yl)methyl)benzof-uro[3, 2-b] quinolin-11-amine (4a-14). Compounds **2a-1** was reacted with tetrahydrofurfurylamine according to general procedure to afford **4a-14** as a yellow solid. Yield 60 %. ^{1}H NMR (400 MHz, $CDCl_3$) δ 8.31 (d, *J* = 7.6 Hz, 1H), 8.09 (d, *J* = 8.8 Hz, 1H), 7.86 (d, *J* = 8.8 Hz, 1H), 7.78 (s, 1H), 7.60 – 7.47 (m, 2H), 7.40 (dd, *J* = 17.7, 7.6 Hz, 3H), 7.23 (q, *J* = 7.9 Hz, 2H), 7.12 (t, *J* = 15.2 Hz, 2H), 5.52 (s, 1H), 4.35 (dd, *J* = 12.0, 6.6 Hz, 2H), 4.07 – 3.97 (m, 1H), 3.89 (dd, *J* = 14.0, 6.7 Hz, 2H), 2.51 (s, 3H), 2.24 – 2.09 (m, 2H), 2.05 – 1.94 (m, 2H). ^{13}C NMR (101 MHz, $CDCl_3$) δ 158.03, 146.73, 137.93, 134.29, 134.21, 134.12, 132.89, 129.92, 129.77, 128.24, 127.76, 126.88, 126.67, 125.17, 123.53, 123.09, 121.97, 119.17, 118.20, 111.81, 78.50, 68.30, 49.41, 28.84, 25.99, 15.79. HRMS (ESI) *m/z*: calcd for $C_{29}H_{26}N_2O_2S$, $[M+H]^+$, 467.1788, found 467.1785. HPLC purity: 95.0%.

(E)-N^1,N^1-diethyl-N^3-(2-(p-(methylthio)styryl)benzofuro[3,2-b]quin-olin-11-yl) propane-1,3-diamine (4a-15). Compounds **2a-1** was reacted with 3-diethylaminopropylamine according to general procedure to afford **4a-15** as a yellow solid. Yield 68 %. ^{1}H NMR (400 MHz, DMSO) δ 8.41 (s, 1H), 8.19 (d, *J* = 7.6

Hz, 1H), 7.96 (s, 2H), 7.73 – 7.64 (m, 2H), 7.57 (d, *J* = 8.0 Hz, 3H), 7.46 (t, *J* = 7.2 Hz, 1H), 7.42 – 7.26 (m, 4H), 4.00 (dd, *J* = 12.2, 6.1 Hz, 2H), 2.62 (t, *J* = 6.2 Hz, 2H), 2.57 – 2.51 (m, 7H), 2.01 – 1.82 (m, 2H), 0.98 (t, *J* = 7.0 Hz, 6H).^{13}C NMR (101 MHz, $CDCl_3$) δ 158.05, 147.06, 146.82, 137.87, 135.69, 134.42, 134.23, 132.28, 129.85, 129.51, 128.00, 127.79, 126.79, 126.72, 125.05, 123.74, 122.83, 121.91, 120.47, 118.40, 111.79, 53.68, 47.45, 47.30, 25.64, 15.82, 11.67. HRMS (ESI) *m/z*: calcd for $C_{31}H_{33}N_3OS$, $[M+H]^+$, 496.2417, found 496.2425. HPLC purity: 99.7%.

(E)-N-(2-(4-methylpiperazin-1-yl)ethyl)-2-(p-(methylthio)styryl)ben-zofuro[3,2-b] quinolin-11-amine (4a-16). Compounds **2a-1** was reacted with 2-(4-methyl-1-piperazinyl) ethanamine according to general procedure to afford **4a-16** as a yellow solid. Yield 72 %. ^{1}H NMR (400 MHz, DMSO) δ 8.41 (s, 1H), 8.19 (d, *J* = 7.6 Hz, 1H), 7.96 (s, 2H), 7.73 – 7.64 (m, 2H), 7.57 (d, *J* = 8.0 Hz, 3H), 7.46 (t, *J* = 7.2 Hz, 1H), 7.42 – 7.26 (m, 4H), 4.00 (dd, *J* = 12.2, 6.1 Hz, 2H), 2.62 (t, *J* = 6.2 Hz, 2H), 2.57 – 2.51 (m, 7H), 2.01 – 1.82 (m, 2H), 0.98 (t, *J* = 7.0 Hz, 6H). ^{13}C NMR (101 MHz, $CDCl_3$) δ 158.20, 146.86, 138.09, 134.54, 134.22, 132.76, 130.04, 129.80, 128.20, 127.89, 126.88, 126.70, 125.60, 123.64, 123.05, 121.97, 118.86, 118.47, 111.86, 56.74, 55.65, 52.65, 46.23, 41.51, 15.78. HRMS (ESI) *m/z*: calcd for $C_{31}H_{32}N_4OS$, $[M+H]^+$, 509.2370, found 509.2372. HPLC purity: 99.7%.

(E)-2-(p-(methylthio)styryl)-N-(3-morpholinopropyl)benzofuro[3,2-b]quinolin-11-amine (4a-17). Compounds **2a-1** was reacted with 3-morpholinopropylamine according to general procedure to afford **4a-17** as a yellow solid. Yield 72 %. ^{1}H NMR (400 MHz, $CDCl_3$) δ 8.24 (d, *J* = 6.0 Hz, 1H), 8.03 (d, *J* = 9.6 Hz, 1H), 7.84 (d,

J = 7.4 Hz, 2H), 7.43 (s, 2H), 7.37 (d, *J* = 8.3 Hz, 2H), 7.30 (t, *J* = 7.3 Hz, 1H), 7.17 (d, *J* = 5.7 Hz, 3H), 7.07 (d, *J* = 16.2 Hz, 1H), 6.75 (s, 1H), 4.14 (dd, *J* = 10.9, 5.4 Hz, 2H), 3.89 – 3.74 (m, 4H), 2.62 – 2.56 (m, 2H), 2.51 (s, 4H), 2.40 (s, 3H), 1.98 – 1.88 (m, 2H). ^{13}C NMR (101 MHz, $CDCl_3$) δ 158.06, 146.89, 146.84, 138.07, 135.13, 134.21, 134.17, 132.64, 130.09, 129.69, 128.35, 127.45, 126.82, 126.75, 124.76, 123.61, 122.98, 121.93, 120.18, 118.26, 111.80, 66.86, 59.08, 54.21, 46.66, 25.25, 15.76. HRMS (ESI) *m/z*: calcd for $C_{31}H_{31}N_2O_2S$, $[M+H]^+$, 510.2210, found 510.2210. HPLC purity: 99.3%.

(E)-2-(p-(methylthio)styryl)-11-morpholinobenzofuro[3,2-b]quino-line (4a-18). Compounds **2a-1** was reacted with morpholine according to general procedure to afford **4a-18** as a yellow solid. Yield 66 %. ^{1}H NMR (400 MHz, $CDCl_3$) δ 8.37 (s, 1H), 8.19 (s, 2H), 7.99 (d, *J* = 8.9 Hz, 1H), 7.70 – 7.58 (m, 2H), 7.53 (d, *J* = 8.1 Hz, 2H), 7.47 (t, *J* = 7.2 Hz, 1H), 7.29 (dd, *J* = 12.2, 7.9 Hz, 3H), 7.25 (s, 1H), 4.13 – 4.04 (m, 4H), 3.70 (s, 4H), 2.53 (s, 3H). ^{13}C NMR (101 MHz, $CDCl_3$) δ 158.69, 147.83, 147.50, 141.58, 138.30, 137.00, 134.10, 134.08, 130.53, 130.05, 128.96, 127.93, 127.02, 126.67, 125.26, 124.04, 123.52, 123.13, 122.58, 122.10, 112.07, 67.59, 52.49, 15.77. HRMS (ESI) *m/z*: calcd for $C_{28}H_{24}N_2O_2S$, $[M+H]^+$, 453.1631, found 453.1634. HPLC purity: 99.8%.

(E)-N1-(2-(p-(methylthio)styryl)benzofuro[3,2-b]quinolin-11-yl)ethan-e-1,2-diamine (4a-19). Compounds **2a-1** was reacted with ethylenediamine according to general procedure to afford **4a-19** as a yellow solid. Yield 78 %. ^{1}H NMR (400 MHz, DMSO) δ 8.52 (s, 1H), 8.18 (d, *J* = 7.7 Hz, 1H), 7.95 (s, 2H), 7.75 (d, *J* = 8.1 Hz,

1H), 7.66 (t, J = 7.7 Hz, 1H), 7.59 (d, J = 8.1 Hz, 2H), 7.45 (dd, J = 12.9, 5.5 Hz, 1H), 7.38 (d, J = 9.1 Hz, 1H), 7.31 (d, J = 8.2 Hz, 2H), 7.25 (s, 1H), 4.02 – 3.93 (m, 2H), 2.96 (t, J = 6.4 Hz, 2H), 2.52 (s, 3H). ^{13}C NMR (101 MHz, $CDCl_3$) δ 158.12, 146.86, 138.00, 134.40, 134.25, 132.90, 130.09, 129.79, 128.29, 127.84, 126.91, 126.71, 125.18, 123.61, 123.07, 121.94, 119.21, 118.36, 111.86, 47.46, 42.05, 15.81. HRMS (ESI) *m/z*: calcd for $C_{26}H_{23}N_3OS$, $[M+H]^+$, 426.1635, found 426.1632. HPLC purity: 99.8%.

(E)-N^1-(2-(p-(methylthio)styryl)benzofuro[3,2-b]quinolin-11-yl)pro-pane-1,3-diamine (4a-20). Compounds **2a-1** was reacted with trimethylenediamine according to general procedure to afford **4a-20** as a yellow solid. Yield 80%. ^{1}H NMR (400 MHz, DMSO) δ 8.49 (s, 1H), 8.18 (d, J = 7.6 Hz, 1H), 7.95 (s, 2H), 7.74 (d, J = 8.2 Hz, 1H), 7.66 (t, J = 7.8 Hz, 1H), 7.59 (d, J = 8.4 Hz, 2H), 7.45 (dd, J = 14.4, 6.9 Hz, 1H), 7.41 – 7.24 (m, 4H), 4.03 (t, J = 6.3 Hz, 2H), 2.81 (t, J = 6.7 Hz, 2H), 2.50 (s, 5H), 1.94 – 1.83 (m, 2H). ^{13}C NMR (101MHz, $CDCl_3$) δ 158.09, 146.96, 146.87, 137.89, 135.18, 134.35, 134.09, 132.51, 129.91, 129.63, 128.08, 127.98, 126.87, 126.72, 125.20, 123.67, 122.93, 121.91, 119.89, 118.36, 111.83, 45.93, 41.40, 32.12, 15.83. HRMS (ESI) *m/z*: calcd for $C_{27}H_{25}N_3OS$, $[M+H]^+$, 440.1791, found 440.1781. HPLC purity: 99.6%.

(E)-N^1,N^1,N^3-trimethyl-N^3-(2-(p-(methylthio)styryl)benzofuro[3,2-b]-quinoli n-11-yl)propane-1,3-diamine (4a-21). Compounds **2a-1** was reacted with *N,N,N*-Trimethyl-1,3-propanediamine according to general procedure to afford **4a-21** as a yellow solid. Yield 60 %. ^{1}H NMR (400 MHz, $CDCl_3$) δ 8.35 (d, J = 7.6 Hz, 1H),

8.25 (s, 1H), 8.19 (d, *J* = 8.9 Hz, 1H), 7.95 (dd, *J* = 8.9, 1.4 Hz, 1H), 7.61 (q, *J* = 8.2 Hz, 2H), 7.51 (d, *J* = 8.3 Hz, 2H), 7.44 (dd, *J* = 10.9, 4.6 Hz, 1H), 7.30 (dd, *J* = 15.9, 12.4 Hz, 3H), 7.22 (d, *J* = 16.3 Hz, 1H), 3.65 (t, *J* = 7.3 Hz, 2H), 3.29 (s, 3H), 2.53 (s, 3H), 2.37 (d, *J* = 7.2 Hz, 2H), 2.19 (s, 6H), 1.89 (dt, *J* = 14.5, 7.4 Hz, 2H). ^{13}C NMR (101 MHz, $CDCl_3$) δ 158.58, 147.65, 147.50, 142.19, 138.62, 138.09, 134.27, 133.79, 130.31, 129.88, 128.63, 128.16, 126.97, 126.72, 125.24, 124.94, 123.39, 123.35, 123.22, 122.07, 112.03, 57.39, 54.28, 45.57, 42.22, 26.36, 15.80. HRMS (ESI) m/z: calcd for $C_{30}H_{31}N_3OS$, $[M+H]^+$, 482.2261, found 482.2255. HPLC purity: 96.7%.

(E)-2-(4-(2-(p-(methylthio)styryl)benzofuro[3,2-b]quinolin-11-yl)pi-perazin-1-yl) ethan-1-ol (4a-22). Compounds **2a-1** was reacted with N-(2-hydroxyethyl)piperazine according to general procedure to afford **4a-22** as a yellow solid. Yield 65 %. ^{1}H NMR (400 MHz, DMSO) δ 8.25 (d, *J* = 7.6 Hz, 1H), 8.19 (s, 1H), 8.11 (s, 2H), 7.80 (d, *J* = 8.3 Hz, 1H), 7.72 (t, *J* = 7.8 Hz, 1H), 7.66 (d, *J* = 8.3 Hz, 2H), 7.53 (dd, *J* = 21.2, 12.0 Hz, 2H), 7.39 (d, *J* = 16.4 Hz, 1H), 7.30 (d, *J* = 8.3 Hz, 2H), 4.52 (s, 1H), 3.63 (t, *J* = 8.6 Hz, 6H), 2.84 (s, 4H), 2.61 (s, 2H), 2.52 (s, 3H). ^{13}C NMR (101 MHz, DMSO) δ 158.48, 147.43, 147.17, 141.10, 138.29, 137.81, 134.32, 134.20, 131.38, 130.18, 129.23, 128.27, 127.69, 126.46, 125.54, 124.27, 123.92, 123.56, 123.08, 122.12, 112.86, 60.87, 59.09, 54.12, 52.32, 15.07. HRMS (ESI) m/z: calcd for C_{30} $H_{29}N_3O_2S$, $[M+H]^+$, 496.2053, found 496.2046. HPLC purity: 98.8%.

(E)-2-(2-((2-(p-(methylthio)styryl)benzofuro[3,2-b]quinolin-11-yl)am-ino)ethoxy) ethan-1-ol (4a-23). Compounds **2a-1** was reacted with

2-(2-aminoethoxy)ethanol according to general procedure to afford **4a-23** as a yellow green solid. Yield 66 %. ^{1}H NMR (400 MHz, DMSO) δ 8.53 (s, 1H), 8.20 (d, J = 7.6 Hz, 1H), 7.97 (s, 2H), 7.75 (d, J = 8.3 Hz, 1H), 7.71 – 7.65 (m, 1H), 7.59 (d, J = 8.4 Hz, 2H), 7.47 (dd, J = 13.6, 6.2 Hz, 1H), 7.40 (s, 1H), 7.36 (s, 1H), 7.31 (d, J = 8.3 Hz, 2H), 4.64 (t, J = 4.6 Hz, 1H), 4.14 (dd, J = 11.7, 5.9 Hz, 2H), 3.82 (t, J = 5.9 Hz, 2H), 3.53 (s, 4H), 2.52 (s, 3H). ^{13}C NMR (101MHz, DMSO) δ 157.81, 146.90, 146.21, 138.34, 138.14, 135.50, 134.29, 133.37, 130.61, 129.75, 128.50, 128.02, 127.33, 126.63, 123.83, 123.59, 121.91, 120.90, 118.64, 112.67, 72.78, 70.68, 60.71, 44.92, 15.07. HRMS (ESI) m/z: calcd for $C_{28}H_{22}N_2O_3S$, $[M+H]^+$, 471.1737, found 471.1722. HPLC purity: 95.0%.

(E)-2-((2-((2-(p-(methylthio)styryl)benzofuro[3,2-b]quinolin-11yl)a-mino)ethyl) amino)ethan-1-ol (4a-24). Compounds **2a-1** was reacted with 2-(2-aminoethylamino)ethanol according to general procedure to afford **4a-24** as a yellow green solid. Yield 67 %. ^{1}H NMR (400 MHz, DMSO) δ 8.50 (s, 1H), 8.19 (d, J = 7.5 Hz, 1H), 7.96 (s, 2H), 7.74 (d, J = 8.2 Hz, 1H), 7.67 (t, J = 7.7 Hz, 1H), 7.59 (d, J = 8.4 Hz, 2H), 7.46 (dd, J = 13.9, 6.6 Hz, 1H), 7.38 (d, J = 8.9 Hz, 1H), 7.31 (d, J = 8.3 Hz, 3H), 4.54 (s, 1H), 4.04 (dd, J = 12.0, 6.1 Hz, 2H), 3.50 (t, J = 5.6 Hz, 2H), 2.99 (t, J = 6.5 Hz, 2H), 2.72 (t, J = 5.7 Hz, 2H), 2.52 (s, 3H).^{13}C NMR (101 MHz, DMSO) δ 157.80, 147.02, 146.24, 145.26, 138.10, 135.65, 134.33, 133.38, 132.60, 129.81, 128.41, 128.10, 127.31, 126.66, 126.45, 123.75, 123.68, 121.87, 121.02, 118.65, 112.63, 60.98, 51.99, 50.29, 45.34, 15.09. HRMS (ESI) m/z: calcd for $C_{28}H_{27}N_3O_2S$, $[M+H]^+$, 470.1897, found 470.1899. HPLC purity: 96.6%.

(E)-2-(p-(methylthio)styryl)-11-(4-(pyridin-2-yl)piperazin-1-yl)benz-ofuro[3, 2-b]quinoline (4a-25). Compounds **2a-1** was reacted with 1-pyridin-2-ylpiperazine according to general procedure to afford **4a-25** as a yellow green solid. Yield 68 %. ^{1}H NMR (400 MHz, $CDCl_3$) δ 8.28 (d, J = 7.7 Hz, 1H), 8.23 – 8.08 (m, 3H), 7.90 (d, J = 8.8 Hz, 1H), 7.58 – 7.46 (m, 3H), 7.43 (d, J = 8.2 Hz, 2H), 7.37 (t, J = 7.3 Hz, 1H), 7.22 (d, J = 18.4 Hz, 3H), 7.14 (d, J = 16.3 Hz, 1H), 6.74 (d, J = 8.6 Hz, 1H), 6.67 – 6.60 (m, 1H), 3.85 (s, 4H), 3.72 (t, J = 4.6 Hz, 4H), 2.44 (s, 3H). ^{13}C NMR (101 MHz, $CDCl_3$) δ 159.71, 158.71, 148.10, 147.80, 147.51, 141.58, 141.56, 138.24, 137.66, 137.29, 134.10, 130.51, 130.03, 128.93, 127.97, 127.03, 126.69, 125.35, 124.11, 123.50, 123.17, 122.68, 122.12, 113.82, 112.08, 107.49, 52.02, 46.18, 15.79. HRMS (ESI) m/z: calcd for C_{33} $H_{28}N_4OS$, $[M+H]^+$, 529.2057, found 529.2047. HPLC purity: 99.9%.

(E)-N-(3-(1H-imidazol-1-yl)propyl)-2-(p-(methylthio)styryl)benzofu-ro[3,2-b] quinolin-11-amine (4a-26). Compounds **2a-1** was reacted with N-(3-aminopropyl)-imidazole according to general procedure to afford **4a-26** as a yellow green solid. Yield 70 %. ^{1}H NMR (400 MHz, $CDCl_3$) δ 8.14 (d, J = 7.6 Hz, 1H), 7.94 (d, J = 8.9 Hz, 1H), 7.71 (d, J = 8.8 Hz, 1H), 7.56 (s, 1H), 7.47 – 7.17 (m, 7H), 7.06 – 6.98 (m, 3H), 6.96 (s, 1H), 6.81 (s, 1H), 4.95 (s, 1H), 4.03 (t, J = 6.7 Hz, 2H), 3.90 (dd, J = 13.5, 6.7 Hz, 2H), 2.32 (s, 3H), 2.22 – 2.13 (m, 2H). ^{13}C NMR (101MHz, $CDCl_3$) δ 158.06, 146.84, 146.58, 138.15, 137.21, 134.06, 133.75, 133.73, 133.19, 130.08, 129.93, 129.85, 128.53, 127.49, 126.88, 126.60, 125.50, 123.29, 121.96, 119.01, 118.89, 118.14, 111.94, 99.99, 44.72, 42.80, 32.59, 15.72. HRMS

(ESI) m/z: calcd for $C_{30}H_{26}N_4OS$, $[M+H]^+$, 491.1900, found 491.1904. HPLC purity: 99.8%.

(E)-N-(2-(4-methylpiperazin-1-yl)ethyl)-3-(4-(methylthio)-styryl)be-nzofuro[3,2-b]quinolin-11-amine (4b-1). Compounds **2b-1** was reacted with 2-(4-methyl-1-piperazinyl)ethanamine according to general procedure to afford **4b-1** as a yellow solid. Yield 72 %. ^{1}H NMR (400 MHz, DMSO) δ 8.30 (d, J = 8.9 Hz, 1H), 8.20 (d, J = 7.5 Hz, 1H), 8.09 (s, 1H), 7.81 (d, J = 8.9 Hz, 1H), 7.76 – 7.55 (m, 4H), 7.45 (dt, J = 24.3, 12.0 Hz, 3H), 7.30 (d, J = 8.1 Hz, 2H), 7.20 (t, J = 5.1 Hz, 1H), 4.02 (dd, J = 11.9, 5.6 Hz, 2H), 2.72 (t, J = 6.6 Hz, 2H), 2.54 (s, 4H), 2.51 (s, 3H), 2.39 (s, 4H), 2.19 (s, 3H).^{13}C NMR (101MHz, DMSO) δ 157.80, 147.77, 146.78, 138.33, 137.22, 135.59, 134.19, 133.17, 130.59, 129.54, 127.78, 127.60, 126.52, 123.75, 123.63, 122.99, 121.95, 121.22, 117.70, 112.59, 100.01, 58.79, 55.15, 53.14, 46.01, 42.38, 15.07. HRMS (ESI) m/z: calcd for $C_{31}H_{32}N_4OS$, $[M+H]^+$, 509.2370, found 509.2390. HPLC purity: 95.3%.

(E)-3-(p-(methylthio)styryl)-N-(2-(pyrrolidin-1-yl)ethyl)-benzofuro-[3,2-b]quinolin-11-amine. (4b-2). Compounds **2b-1** was reacted with 1-(2-aminoethyl)pyrrolidine according to general procedure to afford **4b-2** as a yellow solid. Yield 74 %. ^{1}H NMR (400 MHz, DMSO) δ 8.33 (d, J = 8.9 Hz, 1H), 8.20 (d, J = 7.6 Hz, 1H), 8.08 (s, 1H), 7.81 (d, J = 8.9 Hz, 1H), 7.76 – 7.58 (m, 4H), 7.45 (dt, J = 24.3, 12.0 Hz, 3H), 7.30 (d, J = 7.9 Hz, 3H), 4.05 (dd, J =13.0, 6.5 Hz, 2H), 2.87 (s, 2H), 2.65 (s, 4H), 2.52 (s, 3H), 1.73 (s, 4H).^{13}C NMR (101 MHz, DMSO) δ 157.80, 147.79, 146.81, 138.32, 137.22, 135.48, 134.19, 133.06, 130.58, 129.53, 127.79,

127.75, 127.60, 126.52, 123.75, 123.63, 123.11, 121.95, 121.20, 117.69, 112.60, 56.74, 54.28, 43.94, 23.64, 15.07. HRMS (ESI) m/z: calcd for $C_{30}H_{29}N_3OS$, $[M+H]^+$, 480.2104, found 480.2104. HPLC purity: 99.9%.

(E)-N^1,N^1-dimethyl-N^2-(2-(p-(methylthio)styryl)-10H-indolo[3,2-b]-quinolin-11-yl)ethane-1,2-diamine (4c-1). Compounds **2a-2** was reacted with 2-dimethylaminoethylamine according to general procedure to afford **4c-1** as a yellow solid. Yield 74 %. ^{1}H NMR (400 MHz, DMSO) δ 11.40 (s, 1H), 8.40 (s, 1H), 8.23 (d, J = 7.7 Hz, 1H), 7.99 (d, J = 8.8 Hz, 1H), 7.90 (d, J = 8.9 Hz, 1H), 7.63 – 7.50 (m, 4H), 7.37 (d, J = 3.9 Hz, 2H), 7.31 (d, J = 8.0 Hz, 2H), 7.22 (t, J = 7.2 Hz, 1H), 6.57 (t, J = 28.0 Hz, 1H), 3.91 (dd, J = 11.4, 5.5 Hz, 2H), 2.67 (s, 2H), 2.52 (s, 3H), 2.31 (s, 6H). ^{13}C NMR (101 MHz, DMSO) δ 145.92, 145.28, 143.56, 137.80, 136.04, 134.56, 131.68, 129.88, 128.90, 128.69, 127.62, 127.25, 126.72, 124.38, 122.42, 121.33, 120.97, 120.18, 119.31, 118.01, 112.33, 60.24, 45.90, 44.02, 15.19. HRMS (ESI) m/z: calcd for $C_{28}H_{28}N_4S$, $[M+H]^+$, 453.2107, found 453.2107. HPLC purity: 99.9%.

(E)-N^1,N^1-dimethyl-N^3-(2-(p-(methylthio)styryl)-10H-indolo[3,2-b]-quinolin-11-yl)propane-1,3-diamine (4c-2). Compounds **2a-2** was reacted with 3-dimethylaminopropylamine according to general procedure to afford **4c-2** as a yellow solid. Yield 73 %. ^{1}H NMR (400 MHz, DMSO) δ 11.97 (s, 1H), 8.47 (s, 1H), 8.24 (d, J = 7.7 Hz, 1H), 7.99 (d, J = 8.8 Hz, 1H), 7.88 (d, J = 8.7 Hz, 1H), 7.51-7.58 (m, 4H), 7.36 (s, 2H), 7.30 (d, J = 8.3 Hz, 2H), 7.21 (t, J = 6.6 Hz, 1H), 6.76 (t, J = 6.4 Hz, 1H), 3.87 (dd, J = 12.0, 6.4 Hz, 2H), 2.57 (t, J = 5.9 Hz, 2H), 2.51 (s, 3H),

2.32 (s, 6H), 1.99 – 1.86 (m, 2H). ^{13}C NMR (101 MHz, DMSO) δ 146.01, 145.28, 143.53, 137.80, 136.70, 134.56, 131.60, 129.81, 128.90, 128.68, 127.55, 127.19, 126.73, 124.54, 122.51, 121.34, 120.92, 120.14, 119.21, 118.01, 112.25, 55.68, 44.97, 42.95, 28.03, 15.18. HRMS (ESI) m/z: calcd for $C_{29}H_{30}N_4S$, $[M+H]^+$, 467.2264, found 467.2274. HPLC purity: 95.0%.

(E)-N^1,N^1-diethyl-N^2-(2-(p-(methylthio)styryl)-10H-indolo[3,2-b]qui-nolin-11-yl)ethane-1,2-diamine (4c-3). Compounds **2a-2** was reacted with N,N-diethylethylenediamine according to general procedure to afford **4c-3** as a yellow solid. Yield 73 %. ^{1}H NMR (400 MHz, DMSO) δ 11.77 (s, 1H), 8.40 (s, 1H), 8.23 (d, J = 7.7 Hz, 1H), 7.99 (d, J = 8.9 Hz, 1H), 7.88 (d, J = 8.0 Hz, 1H), 7.61 – 7.51 (m, 4H), 7.36 (s, 2H), 7.31 (d, J = 8.3 Hz, 2H), 7.24 – 7.19 (m, 1H), 6.68 (t, J = 6.0 Hz, 1H), 3.89 (dd, J = 11.5, 5.7 Hz, 2H), 2.81 (t, J = 5.7 Hz, 2H), 2.65 (q, J = 7.0 Hz, 4H), 2.52 (s, 3H), 1.00 (t, J = 7.1 Hz, 6H). ^{13}C NMR (101 MHz, DMSO) δ 145.91, 145.25, 143.47, 137.83, 136.21, 134.54, 131.61, 129.83, 128.91, 128.62, 127.61, 127.21, 126.73, 124.59, 122.57, 121.39, 120.61, 120.16, 119.28, 117.89, 112.16, 54.35, 47.58, 44.48, 15.18, 11.98. HRMS (ESI) m/z: calcd for $C_{30}H_{32}N_4S$, $[M+H]^+$, 481.2420, found 481.2428. HPLC purity: 97.1%.

(E)-N^1,N^1-diethyl-N^3-(2-(p-(methylthio)styryl)-10H-indolo[3,2-b]qui-nolin-11-yl)propane-1,3-diamine (4c-4). Compounds **2a-2** was reacted with 3-diethylaminopropylamine according to general procedure to afford **4c-4** as a yellow solid. Yield 73 %. ^{1}H NMR (400 MHz, DMSO) δ 11.34 (s, 1H), 8.42 (s, 1H), 8.23 (d, J = 7.7 Hz, 1H), 7.97 (d, J = 8.8 Hz, 1H), 7.88 (d, J = 8.7 Hz, 1H), 7.55 (t, J = 8.7 Hz,

4H), 7.38 – 7.27 (m, 4H), 7.21 (t, *J* = 6.4 Hz, 1H), 6.85 (s, 1H), 3.90 (dd, *J* = 12.3,6.4 Hz, 2H), 2.62 (dt, *J* = 14.0, 6.4 Hz, 6H), 2.51 (s, 3H), 2.00 – 1.84 (m, 2H), 0.98 (t, *J* = 7.0 Hz, 6H). ^{13}C NMR (101MHz, DMSO) δ 146.06, 145.38, 143.40, 137.83, 136.56, 134.56, 131.56, 129.86, 128.90, 128.62, 127.56, 127.17, 126.75, 124.49, 122.59, 121.35, 121.06, 119.76, 119.31, 117.89, 112.18, 49.53, 46.82, 43.65, 27.90, 15.18, 11.46.HRMS (ESI) m/z: calcd for C_{31} $H_{34}N_4S$, $[M+H]^+$, 495.2577, found 495.2566. HPLC purity: 95.1%.

(E)-N-(2-(4-methylpiperazin-1-yl)ethyl)-2-(p-(methylthio)styryl)-10-H-indolo [3,2-b]quinolin-11-amine (4c-5). Compounds **2a-2** was reacted with 2-(4-methyl-1-piperazinyl)ethanamine according to general procedure to afford **4c-5** as a yellow solid. Yield 73 %. ^{1}H NMR (400 MHz, DMSO) δ 11.17 (s, 1H), 8.40 (s, 1H), 8.23 (d, *J* = 7.7 Hz, 1H), 7.98 (d, *J* = 8.8 Hz, 1H), 7.90 (d, *J* = 9.1 Hz, 1H), 7.64 – 7.51 (m, 4H), 7.38 (s, 2H), 7.31 (d, *J* = 8.3 Hz, 2H), 7.22 (t, *J* = 7.2 Hz, 1H), 6.56 (s, 1H), 3.91 (dd, *J* = 11.6, 5.8 Hz, 2H), 2.70 (t, *J* = 5.9 Hz, 2H), 2.52 (s, 7H), 2.35 (s, 4H), 2.13 (s, 3H). ^{13}C NMR (101MHz, DMSO) δ 145.74, 145.08, 143.48, 137.89, 136.23, 134.48, 131.74, 129.69, 129.00, 128.57, 127.71, 127.23, 126.67, 124.71, 122.38, 121.40, 120.78, 120.32, 119.44, 118.18, 112.36, 58.30, 55.18, 53.34, 46.16, 43.42, 15.13. HRMS (ESI) m/z: calcd for C_{31} $H_{33}N_5S$, $[M+H]^+$, 508.2529, found 508.2528. HPLC purity: 98.6%.

(E)-2-(p-(methylthio)styryl)-N-(2-(pyrrolidin-1-yl)ethyl)-10H-indolo-[3,2-b] quinolin-11-amine (4c-6). Compounds **2a-2** was reacted with 1-(2-aminoethyl)pyrrolidine according to general procedure to afford **4c-5** as a yellow

solid. Yield 75 %. ^{1}H NMR (400 MHz, DMSO) δ 11.48 (s, 1H), 8.43 (s, 1H), 8.22 (d, J = 7.7 Hz, 1H), 7.98 (d, J = 8.9 Hz, 1H), 7.89 (d, J = 8.9 Hz, 1H), 7.56 (dd, J = 16.0, 6.8 Hz, 4H), 7.36 (s, 2H), 7.30 (d, J = 8.3 Hz, 2H), 7.21 (dt, J = 13.2, 4.1 Hz, 1H), 6.64 (t, J = 6.1 Hz, 1H), 3.93 (dd, J = 12.1, 6.0 Hz, 2H), 2.84 (t, J = 6.1 Hz, 2H), 2.61 (s, 4H), 2.51 (s, 3H), 1.73 (s, 4H). ^{13}C NMR (101 MHz, DMSO) δ 145.94, 145.29, 143.52, 137.83, 136.11, 134.53, 131.66, 129.85, 128.96, 128.64, 127.60, 127.22, 126.69, 124.54, 122.47, 121.37, 120.89, 120.24, 119.32, 118.07, 112.20, 56.79, 54.43, 45.02, 23.73, 15.14. HRMS (ESI) m/z: calcd for $C_{30}H_{30}N_4S$, $[M+H]^+$, 479.2264, found 479.2279. HPLC purity: 95.7%.

(E)-N-(2-(4-methylpiperazin-1-yl)ethyl)-3-(p-(methylthio)styryl)-10-H-indolo [3,2-b]quinolin-11-amine (4d-1). Compounds **2b-2** was reacted with 2-(4-methyl-1-piperazinyl)ethanamine according to general procedure to afford **4d-1** as a yellow solid. Yield 75%. ^{1}H NMR (400 MHz, DMSO) δ 11.30 (s, 1H), 8.30 (dd, J = 11.9, 8.5 Hz, 2H), 8.11 (d, J = 1.4 Hz, 1H), 7.81 (d, J = 7.9 Hz, 1H), 7.64 (d, J = 8.5 Hz, 3H), 7.58 (t, J = 7.5 Hz, 1H), 7.44 (s, 2H), 7.31 (d, J = 8.4 Hz, 2H), 7.25 (t, J = 7.3 Hz, 1H), 6.79 (s, 1H), 3.94 (dd, J = 11.4, 5.5 Hz, 2H), 2.72 (t, J = 5.9 Hz, 2H), 2.56 (s, 3H), 2.52 (s, 4H), 2.41 (s, 4H), 2.20 (s, 3H). ^{13}C NMR (101 MHz, DMSO) δ 144.74, 144.57, 143.35, 138.19, 137.27, 136.27, 134.27, 129.26, 129.12, 128.02, 127.55, 126.55, 122.73, 121.65, 121.34, 120.58, 119.70, 119.58, 116.92, 112.55, 99.99, 58.19, 54.89, 53.03, 45.81, 43.41, 15.13. HRMS (ESI) m/z: calcd for $C_{31}H_{33}N_5S$, $[M+H]^+$, 508.2529, found 508.2523. HPLC purity: 97.3%.

(E)-3-(p-(methylthio)styryl)-N-(2-(pyrrolidin-1-yl)ethyl)-10H-indolo[3,2-b]

quinolin-11-amine (4d-2). Compounds **2b-2** was reacted with 1-(2-aminoethyl)pyrrolidine according to general procedure to afford **4d-2** as a yellow solid. Yield 78%. ^{1}H NMR (400 MHz, DMSO) δ 11.49 (s, 1H), 8.27 (dd, J = 19.2, 8.4 Hz, 2H), 8.11 (d, J = 1.4 Hz, 1H), 7.80 – 7.72 (m, 1H), 7.62 (d, J = 8.4 Hz, 2H), 7.58 – 7.50 (m, 2H), 7.42 (s, 2H), 7.29 (d, J = 8.4 Hz, 2H), 7.22 (ddd, J = 7.9, 6.7, 4.0 Hz, 1H), 6.60 (t, J = 6.0 Hz, 1H), 3.90 (dd, J = 12.1, 6.0 Hz, 2H), 2.82 (t, J = 6.1 Hz, 2H), 2.60 (s, 4H), 2.51 (s, 3H), 1.72 (s, 4H). ^{13}C NMR (101MHz, DMSO) δ 146.46, 145.85, 143.48, 138.01, 136.09, 135.50, 134.41, 128.99, 128.56, 128.29, 128.01, 127.49, 126.56, 122.52, 122.36, 121.44, 120.29, 120.06, 119.30, 117.31, 112.23, 56.73, 54.40, 44.92, 23.71, 15.11. . HRMS (ESI) m/z: calcd for $C_{30}H_{30}N_4S$, $[M+H]^+$, 479.2264, found 479.2279. HPLC purity: 96.6%.

(E)-5-methyl-2-(p-(methylthio)styryl)-11-((2-(pyrrolidin-1-yl)ethyl)am-ino) benzofuro[3,2-b]quinolin-5-ium iodide (5a-10). Compounds **3a-1** was reacted with 1-(2-aminoethyl)pyrrolidine according to general procedure to afford **5a-10** as an orange solid. Yield 79%. ^{1}H NMR (400 MHz, DMSO) δ 8.89 (s, 1H), 8.67 (d, J = 8.1 Hz, 1H), 8.43 (d, J = 9.2 Hz, 1H), 8.33 (d, J = 9.1 Hz, 1H), 8.01 (d, J = 8.4 Hz, 1H), 7.95 (t, J = 7.7 Hz, 1H), 7.74 – 7.56 (m, 4H), 7.37 (d, J = 16.6 Hz, 1H), 7.32 (d, J = 8.2 Hz, 2H), 4.62 (s, 3H), 4.43 (s, 2H), 2.51 (d, J = 4.1 Hz, 9H), 1.91 (s, 4H). ^{13}C NMR (101 MHz, DMSO) δ 159.02, 157.25, 142.41, 139.17, 138.64, 137.80, 135.04, 133.49, 133.30, 132.24, 131.90, 131.17, 127.64, 126.47, 125.92, 125.48, 125.20, 121.35, 119.04, 117.59, 117.46, 113.66, 54.35, 38.22, 23.67, 14.90. HRMS (ESI) m/z: calcd for $C_{31}H_{31}N_3OS$, $[M-I]^+$, 494.2261, found 494.2272. HPLC purity: 95.4%.

(E)-5-methyl-11-((2-(4-methylpiperazin-1-yl)ethyl)amino)-2-(4-(meth-ylthio)st yryl) benzofuro[3,2-b]quinolin-5-ium iodide (5a-16). Compounds **3a-1** was reacted with 2-(4-methyl-1-piperazinyl)ethanamine according to general procedure to afford **5a-16** as an orange solid. Yield 80%. ^{1}H NMR (400 MHz, DMSO) δ 9.88 (s, 1H), 8.95 (s, 1H), 8.58 (d, J = 7.9 Hz, 1H), 8.27 (d, J = 8.6 Hz, 1H), 8.17 (d, J = 8.5 Hz, 1H), 7.88 (dd, J = 20.5, 8.2 Hz, 2H), 7.69 – 7.45 (m, 4H), 7.35 – 7.17 (m, 3H), 4.51 (s, 3H), 4.24 (d, J = 5.2 Hz, 2H), 2.84 – 2.76 (m, 2H), 2.60 (s, 4H), 2.51 (s, 3H), 2.29 (s, 4H), 2.12 (s, 3H). ^{13}C NMR (101 MHz, DMSO) δ 156.96, 142.62, 138.90, 137.90, 137.72, 134.69, 133.55, 132.88, 132.30, 131.76, 130.82, 130.80, 127.50, 126.35, 125.73, 125.17, 125.03, 121.70, 118.59, 117.47, 113.47, 58.56, 55.26, 53.35, 46.19, 43.66, 37.96, 14.94.HRMS (ESI) m/z: calcd for C_{32} $H_{34}N_4OS$, $[M-I]^+$, 523.2526, found 523.2506. HPLC purity: 98.6%.

(E)-5-methyl-11-((2-(4-methylpiperazin-1-yl)ethyl)amino)-3-(p-(methylthio) styryl)benzofuro[3,2-b]quinolin-5-ium iodide (5b-1). Compounds **3b-1** was reacted with 2-(4-methyl-1-piperazinyl) ethanamine according to general procedure to afford **5b-1** as an orange solid. Yield 80%. ^{1}H NMR (400 MHz, DMSO) δ 9.17 (s, 1H), 8.64 (d, J = 7.6 Hz, 1H), 8.55 (d, J = 8.0 Hz, 1H), 8.26 (s, 1H), 7.98 (d, J = 7.9 Hz, 1H), 7.91 (s, 2H), 7.64 (s, 1H), 7.52 (dd, J = 21.1, 12.0 Hz, 3H), 7.37 (d, J = 16.1 Hz, 1H), 7.19 (d, J = 7.1 Hz, 2H), 4.55 (s, 3H), 4.15 (s, 2H), 3.13 (s, 4H), 2.87 (s, 4H), 2.75 (s, 5H), 2.47 (s, 3H). ^{13}C NMR (101 MHz, DMSO) δ 157.06, 142.67, 142.23, 139.56, 139.01, 138.81, 133.12, 132.91, 131.91, 127.73, 126.08, 125.88, 125.40, 125.14, 124.73, 123.21, 117.26, 115.82, 115.54, 113.62, 57.32, 53.42, 50.48, 43.09, 43.01,

38.31, 14.84.calcd for $C_{32}H_{34}N_4OS$, $[M-I]^+$, 523.2526, found 523.2514. HPLC purity: 98.6%.

(E)-5-methyl-3-(p-(methylthio)styryl)-11-((2-(pyrrolidin-1-yl)ethyl)-amino) benzofuro[3,2-b]quinolin-5-ium iodide (5b-2). Compounds **3b-1** was reacted with 1-(2-aminoethyl)pyrrolidine according to general procedure to afford **5b-2** as an orange solid. Yield 80%. ^{1}H NMR (400 MHz, DMSO) δ 9.31 (s, 1H), 8.67 (d, J = 8.2 Hz, 1H), 8.61 (d, J = 8.9 Hz, 1H), 8.36 (s, 1H), 8.08 (d, J = 8.6 Hz, 1H), 8.00 – 7.87 (m, 2H), 7.76 – 7.58 (m, 4H), 7.50 (d, J = 16.4 Hz, 1H), 7.32 (d, J = 8.1 Hz, 2H), 4.57 (s, 3H), 4.21 (t, J = 5.9 Hz, 2H), 2.92 (s, 2H), 2.64 (s, 4H), 2.52 (s, 3H), 1.72 (s, 4H). ^{13}C NMR (101 MHz, DMSO) δ 157.04, 142.60, 142.33, 139.65, 139.09, 138.73, 133.17, 133.11, 133.02, 131.97, 127.77, 126.21, 126.01, 125.35, 125.09, 124.71, 123.13, 117.32, 115.72, 113.55, 56.18, 54.26, 44.98, 38.08, 23.71, 14.84. HRMS (ESI) m/z: calcd for $C_{31}H_{31}N_3OS$, $[M-I]^+$, 494.2261 found 494.2268. HPLC purity: 96.8%.

(E)-5-methyl-11-((2-(4-methylpiperazin-1-yl)ethyl)amino)-2-(4-(me-thylthio) styryl)-10H-indolo[3,2-b]quinolin-5-ium iodide (5c-5). Compounds **3a-2** was reacted with 2-(4-methyl-1-piperazinyl) ethanamine according to general procedure to afford **5c-5** as a red solid. Yield 82%. ^{1}H NMR (400 MHz, DMSO) δ 12.66 (s, 1H), 8.80 (s, 1H), 8.70 (s, 1H), 8.56 (d, J = 8.4 Hz, 1H), 8.35 (d, J = 9.3 Hz, 1H), 8.24 (d, J = 9.1 Hz, 1H), 7.85 (d, J = 8.4 Hz, 1H), 7.80 – 7.71 (m, 1H), 7.59 (d, J = 8.3 Hz, 2H), 7.51 (d, J = 16.4 Hz, 1H), 7.43 – 7.27 (m, 4H), 4.62 (s, 3H), 4.22 (t, J = 5.1 Hz, 2H), 2.89 (t, J = 5.5 Hz, 2H), 2.62 (s, 3H), 2.51 (s, 4H), 2.34 (s, 4H), 2.14 (s, 3H). ^{13}C NMR (101 MHz, DMSO) δ 144.01, 143.05, 138.87, 136.89, 135.61, 133.65, 130.85,

130.31, 127.51, 126.51, 126.27, 124.86, 121.27, 121.10, 118.44, 117.73, 116.10, 115.52, 114.05, 100.00, 57.58, 54.80, 53.30, 45.90, 43.99, 38.57, 14.97. HRMS (ESI) m/z: calcd for $C_{32}H_{35}N_5S$, $[M-I]^+$, 522.2686 found 522.2690. HPLC purity: 95.3%.

(E)-5-methyl-2-(p-(methylthio)styryl)-11-((2-(pyrrolidin-1-yl)ethyl)-amino)-10H-indolo[3,2-b]quinolin-5-ium iodide (5c-6). Compounds **3a-2** was reacted with 1-(2-aminoethyl)pyrrolidine according to general procedure to afford **5c-6** as a red solid. Yield 80%. ^{1}H NMR (400 MHz, DMSO) δ 11.84 (s, 1H), 8.91 (s, 1H), 8.72 (s, 1H), 8.55 (d, J = 8.3 Hz, 1H), 8.34 (d, J = 9.2 Hz, 1H), 8.24 (d, J = 8.8 Hz, 1H), 7.73 (s, 2H), 7.58 (d, J = 8.0 Hz, 2H), 7.50 (d, J = 16.5 Hz, 1H), 7.41 – 7.21 (m, 4H), 4.62 (s, 3H), 4.25 (s, 2H), 3.17 (s, 2H), 2.81 (s, 4H), 2.51 (s, 3H), 1.78 (s, 4H). ^{13}C NMR (101 MHz, DMSO) δ 143.94, 143.54, 138.89, 138.84, 136.80, 133.70, 133.58, 131.03, 130.73, 130.26, 130.18, 127.50, 126.51, 126.26, 124.81, 121.07, 118.39, 115.99, 115.54, 113.91, 54.49, 38.55, 23.71, 14.99. HRMS (ESI) m/z: calcd for $C_{31}H_{32}N_4S$, $[M-I]^+$, 493.2420, found 493.2404. HPLC purity: 97.5%.

(E)-5-methyl-11-((2-(4-methylpiperazin-1-yl)ethyl)amino)-3-(4-(me-thylthio) styryl)-10H-indolo[3,2-b]quinolin-5-ium iodide (5d-1). Compounds **3b-2** was reacted with 2-(4-methyl-1-piperazinyl) ethanamine according to general procedure to afford **5d-1** as a red solid. Yield 82%. ^{1}H NMR (400 MHz, DMSO) δ 12.51 (s, 1H), 8.74 (s, 1H), 8.59 (d, J = 8.4 Hz, 2H), 8.36 (s, 1H), 8.02 (d, J = 8.8 Hz, 1H), 7.86 (d, J = 8.4 Hz, 1H), 7.79 – 7.49 (m, 5H), 7.39 (t, J = 7.7 Hz, 1H), 7.33 (d, J = 8.4 Hz, 2H), 4.64 (s, 3H), 4.19 (s, 2H), 2.87 (t, J = 5.4 Hz, 2H), 2.62 (s, 4H), 2.53 (s, 3H), 2.37 (d, J = 39.5 Hz, 4H), 2.21 (s, 3H). ^{13}C NMR (101 MHz, DMSO) δ 144.05,

142.85, 141.64, 139.48, 138.29, 135.81, 133.49, 132.64, 130.84, 127.85, 126.64, 126.40, 124.83, 124.49, 121.91, 121.20, 117.54, 115.57, 115.41, 114.59, 114.05, 57.45, 54.62, 52.93, 45.62, 43.86, 38.47, 14.91. HRMS (ESI) m/z: calcd for $C_{32}H_{35}N_5S$, $[M-I]^+$, 522.2686, found 522.2675. HPLC purity: 94.7%.

(E)-5-methyl-3-(p-(methylthio)styryl)-11-((2-(pyrrolidin-1-yl)ethyl)-amino)-10H-indolo[3,2-b]quinolin-5-ium iodide (5d-2). Compounds **3b-2** was reacted with 1-(2-aminoethyl)pyrrolidine according to general procedure to afford **5d-2** as a red solid. Yield 81%. ^{1}H NMR (400 MHz, DMSO) δ 8.88 (s, 1H), 8.60 (d, J = 5.4 Hz, 2H), 8.39 (s, 1H), 8.06 (d, J = 4.5 Hz, 1H), 7.83 – 7.49 (m, 6H), 7.46 – 7.23 (m, 3H), 4.66 (s, 3H), 4.18 (s, 2H), 3.08 (s, 2H), 2.73 (s, 4H), 2.53 (s, 3H), 1.75 (s, 4H).^{13}C NMR (101 MHz, DMSO) δ 144.00, 143.27, 141.48, 139.43, 138.15, 135.73, 133.46, 132.53, 130.83, 127.81, 126.62, 126.35, 124.78, 124.33, 121.74, 120.94, 118.08, 118.00, 115.54, 115.49, 114.42, 113.88, 56.02, 54.43, 44.90, 38.39, 23.76, 14.89. HRMS (ESI) m/z: calcd for $C_{31}H_{32}N_4S$, $[M-I]^+$, 493.2420, found 493.2425. HPLC purity: 96.8%.

Materials in Biological Assay. All oligomers/primers used in this study were purchased from Life Technologies (Beijing, China). Stock solutions of all the compounds (10 mM) were made using DMSO and stored at -20 ^{o}C. Further dilutions to working concentrations were made with relevant buffer before use.

Surface Plasmon Resonance (SPR) Biosensor Measurements. SPR measurements were performed on a ProteOn^{TM} XPR36 Protein Interaction Array system (Bio-Rad Laboratories, Hercules, CA) using a neutravidin-coated NLC sensor

chip. In a typical experiment, biotin NRQ, biotin-NRQ_mutant, and biotin-hairpin oligomers (**Supplementary Table S1**) were folded in a running buffer (Tris-HCl 50 mM pH7.4, 150 mM KCl, 0.005% Tween-20). The samples were then immobilized (1,000 RU) in flow cells, and a blank cell was set as a control. Compound solutions (with the concentrations of 0.3125, 0.625, 1.25, 2.5, 5, 10, and 20 μM) were prepared within the running buffer by serial dilutions from stock solutions. The NLC sensor chip was regenerated with a short injection of NaOH solution between consecutive measurements. The final graphs were obtained by subtracting blank sensorgrams from the NRQ, NRQ-mutant, or hairpin sensorgrams. The data were analyzed with ProteOn™ manager software, using an equilibrium model to fit the kinetic data: K_D = ([A]×[B]) / [AB]. Here, [AB] is the concentration of the complex, [A] and [B] are the concentrations of analyte and the substance, respectively. All of the experiments were repeated for two times.

MTT assay. Human melanoma cells A375, human lung adenocarcinoma cells A549, human cervical cancer cells Hela, human hepatoma cells Huh7, human colon cancer cells HCT116, human breast cancer cells MCF-7, and human normal colon mucosal epithelial cells NCM460 were seeded on 96-well plates (5 000 cells/well) and treated with test compounds at various concentrations. After 48-h treatment at 37 ^{o}C in a humidified atmosphere of 5% CO_2, 20 μL of 2.5 mg/mL 3-(4,5-dimethyl-2-thiazolyl)-2,5-diphenyl-2-H-tetrazolium bromide (MTT) solution was added to each well and further incubated for 4 h. The cells in each well were then treated with DMSO (200 μL for each well) and the optical density (OD) was recorded

at 570 nm. The cytotoxicity was evaluated based on the percentage of cell survival in a dose-dependent manner regard to the blank. The final IC_{50} values were calculated by using the GraphPad Prism 6.0. All of the experiments were repeated for three times.

Circular dichroism spectroscopy (CD). CD studies were performed on a Chirascan circular dichroism spectrophotometer (Applied Photophysics, UK). A quartz cuvette with a 4-mm path length was used for the recording of spectra over a wavelength range of 230-450 nm with a 1 nm bandwidth, 1 nm step size and time of 0.5 s per point. The RNA oligomers (**Supplementary Table S1**) were set at the concentration of 5 μM and pre-annealed with the compounds in a 10 mM Tris-HCl buffer (pH 7.4, in the absence or presence of 100 mM KCl). A buffer baseline was collected in the same cuvette and subtracted from the sample spectra. In a melting experiment, the spectrum was recorded at increasing temperature from 25 to 95 ^{o}C and DNA or RNA oligomers were pre-annealed with compounds in a 10 mM Tris-HCl buffer (pH 7.4, 0.2, 0.5, or 10 mM KCl). Temperature increasing at the rate of 2 ^{o}C/min and curves collected with an interval of 5 ^{o}C. All final analysis of the data was conducted using GraphPad Prism 6.0. All of the experiments were repeated for two times.

Ultraviolet (UV) titration. Absorption spectra were performed on a Shimadzu UV-2450 spectrophotometer using a quartz cuvette with 1-cm path length at room temperature. Compound solutions were prepared in a Tris-HCl buffer (10 mM Tris-HCl, 100 mM KCl, pH 7.4) to a final concentration of 5 μM and the spectra was recorded after each addition of concentrated pre-annealed NRQ oligomer

(**Supplementary Table S1**) into the solution over a wavelength range of 220-700 nm. Final analysis of the data was conducted using GraphPad Prism 6.0.

Fluorescent Titration and Job's plot assay. Fluorescence spectra was performed on a Horiba FluoroMax-4 spectrophotometer at room temperature using a quartz cuvette of 1-cm path length. For a titration assay, compound solutions were prepared using a Tris-KCl buffer (10 mM Tris-HCl,100 mM KCl, pH 7.4) to a final concentration of 1 μM and the spectra was recorded after each addition of concentrated pre-annealed NRQ oligomer (**Supplementary Table S1**) into the solution. For the Job's plot assay, the total compound/quadruplex system was kept at 1 μM in a Tris-KCl buffer (10 mM Tris-HCl,100 mM KCl, pH 7.4), and different scales of compound/NRQ were prepared from 0.05/0.95 to 0.9/0.1. The spectra were recorded over a wavelength range of 450-700 nm, 1 nm step size, and emission at 430 nm. Final analysis of the data was conducted using GraphPad Prism 6.0. All of the experiments were repeated for two times.

Dual-luciferase reporter assay. For this assay, 100 ng of constructed psiCHECK2 plasmid (Clontech, USA) containing WT *NRAS* 5'-UTR or mutant *NRAS* 5'-UTR (**Supplementary Table S1**) and 200 ng of controlled plasmid (Promega, USA) was co-transfected into MCF-7 cells using Lipofectamine 3000 (Invitrogen, USA). After 4 h, **4a-10** were added to the cells at concentrations ranging from 0.125 to 0.5 μM. The cells were incubated at 37 °C with CO_2 for another 48 h, and the transfected cells were first washed with ice-cold PBS to reduce the background signals from the medium. Luciferase assays were subsequently performed according

to the manufacturer's instructions using the Ready-To-Glow Secreted Luciferase Reporter System (Clontech, USA). After a 3-s delay, secreted luciferase signals were collected for 10 s using a microplate reader (Molecular Devices, Flex Station 3, USA), and *Firefly* signals were collected for 10 s as an internal control. The quantification was performed using a multimode reader (Molecular Devices). The secreted *Renilla* activity was normalized to the *Firefly* luciferase activity. Final analysis of the data was conducted using GraphPad Prism 6.0. All of the experiments were repeated for three times.

RNA extraction, RT-PCR and Quantitative Real-time PCR (qPCR). For this assay, different concentration of **4a-10** (0, 0.5, 1.0, and 2.0 μM) were added to A375 cells for 6 h. Then total RNA was isolated by using HiPure Total RNA Mini Kit (Mangen, China). After that, 2 μg of total RNA was reverse transcribed to cDNA by using reverse transcriptase (GenStar, China). The reactions were incubated at 37 °C for 60 min and heated at 99 °C for 5 min to inactivate the transcriptase.[59] The cDNA was further used as a template for PCR amplification using the following condition: melting at 95 °C for 1 min, annealing at 50 °C for 1 min, and extension at 72 °C for 1 min for 30 cycles.

Quantitative PCR was performed with SYBR Premix Ex Taq™ (Takara) and carried out on an ABI PRISM 7900HT Sequence Detection System as the followed cycle conditions: 95 °C denaturing (5 s, first cycle of 30 s), 60 °C annealing and extension (30 s), total 50 cycles. Relative quantification for *NRAS* gene was performed against a house keeping gene *β-actin* according to $2^{-\Delta\Delta Ct}$ method

(**Supplementary Figure S8**).

The primers used in RT-PCR and qRT-PCR, including *NRAS*-A, *NRAS*-S, *β-actin*-A, and *β-actin*-S were shown in **Supplementary Table S1**.

Western Blot Analysis. For this assay, cells treated with different concentration of **4a-10** or **4a-16** for 6 h. Then the cells were collected from 6-well plates and lysed using a RIPA lysis buffer. The whole-cell lysates were separated on a sodium dodecyl sulfate polyacrylamide gel electrophoresis (SDS-PAGE) and transferred to nitrocellulose membranes. After blocking in 5% bull serum albumin (BSA), the membranes were incubated by the primary antibodies, mouse anti-human NRAS (#ab55391, abcam, USA) and rabbit anti-human GAPDH (#2118, CST, USA), and the secondary antibodies. Finally, the membranes were detected by ECL Plus kit. The protein bands were visualized using chemiluminescence substrate.

RNA Immunoprecipitation (RIP). A375 cells were treated with 2-μM **4A-10** or normal Dulbecco's modified eagle medium (DMEM) for 24 h at 37 °C with CO_2. At the end of incubation, 18.5% formaldehyde was added to each dish to obtain a final concentration of 1% formaldehyde, and the treated cells were incubated at 25 °C for 10 min followed by the addition of glycine solution. The cells were detached by scraping after adding 1 mL of ice-cold phosphate-buffered saline (PBS) containing 10 μL of the halt cocktail (Thermo Scientific, USA). Then, 100 μL of RIP Lysis buffer (25-mM Tris-HCl, 150-mM KCl, 2-mM EDTA, 1-mM NaF, 1-mM dithiothreitol [DTT], 0.5% NP-40, pH 7.5) containing the halt cocktail and 100-U/mL RNasin Ribonuclease Inhibitor (Takara, China) were added to the cell pellet and incubated on

ice for 10 min. Next, 100 μL of the supernatant was transferred to 400 μL of immunoprecipitation (IP) dilution buffer (Thermo Scientific, USA) containing protease inhibitors and the RNasin ribonuclease inhibitor. For each IP, 500 μL of diluted lysate was added to protein A/G plus agarose beads with 5 μg of antibody against the DHX36 epitope (#ab70269, abcam) and incubated at 4 °C for 12 h. After centrifugation at 2,000 g for 30 s, the beads were washed with low-salt washing buffer (50-mM Tris-HCl, 150-mM NaCl, 1-mM $MgCl_2$, 2-mM ethylene diamine tetraacetic acid (EDTA), 1-mM dithiothreitol (DTT), 100-U/mL RNase inhibitor, pH 7.4) twice and high-salt washing buffer (50-mM Tris-HCl, 300-mM NaCl, 1-mM $MgCl_2$, 2-mM EDTA, 1-mM DTT, 100-U/mL RNase inhibitor, pH 7.4) twice. Then, 150 μL of IP elution buffer (Thermo, USA) with 6 μL of 5-M NaCl and 2 μL of 20-mg/mL proteinase K were added and incubated at 65 °C for 30 min. The obtained total RNA samples were used for the RT-PCR detection.

Cell cycle arrest assay. The A375 cells were treated with varies concentration of **4a-10** in 10% FBS-supplemented DMEM culture medium at 37 ^{o}C and 5% CO_2 for 24 h. Subsequently, cells were collected and washed with ice-cold PBS and fixed with ice-cold 70% ethanol at -20 ^{o}C overnight. Fixed cells were then washed with PBS again, re-suspended in 0.5 mL of PBS containing 50 mg/mL propidium iodide, and incubated for 30 min in dark. The cell cycle distribution was analyzed by using the EPICS® XL™ flow cytometer within 1 h and calculated by using EXPO 32 software.

Confocal microscopy. A375 cells were treated with 0.25 μM **4a-10** for 6 h at

37 °C and 5% CO_2. After incubation, medium was discarded, cells were washed with PBS for three times to remove the excess compound and then fixed with 4% polyoxymethylene for 15 min. Then, cells were dyed with 4',6-diamidino-2-phenylindole (DAPI, Invitrogen) for 15 min in dark. After that, cells were washed with PBS for three times gently and re-submerged by PBS buffer. Localization of **4a-10** was imaged under a FV3000 laser scanning confocal microscope (Olympus Corporation).

■ AUTHOR INFORMATION

Corresponding Author

* For Tian-Miao Ou: phone, 8620-39943053; e-mail, outianm@mail.sysu.edu.cn.

Notes

The authors declare no competing financial interest.

■ FUNDING

This work was supported by the National Natural Science Foundation of China (Grants 81673286 for T.-M.O.; Grant 81330077 for Z.-S.H.), the Guangdong Provincial Science and Technology Development Special Foundation (Grant 2016A020217006 for T.-M.O.), and the Natural Science Foundation of Guangdong Province (2017A030308003) for financial support of this study.

■ ABBREVIATIONS

NRAS, neuroblastoma RAS; UTR, untranslated region; nt, nucleotide; SPR, surface plasmon resonance; K_D, dissociation constant; MTT, methyl thiazolyl tetrazolium; CD, circular dichroism; T_m, melting temperature; UV-vis, ultraviolet-visible; PAGE, polyacrylamide gel electrophoresis; RT-PCR, reverse transcription-polymerase chain reaction; qRT-PCR, quantitative real-time polymerase chain reaction; RIP, RNA immunoprecipitation assay; MS, mass spectra; HRMS, high resolution mass spectra; m.p., melting points.

■ ASSOCIATED CONTENT

Supporting Information

Additional experimental results, ^{1}H and ^{13}C NMR spectra, HRMS, HPLC assay data for final compounds, and the Molecular Formula Strings are available free of charge via the Internet at http://pubs.acs.org.

■ REFERENCES

1. Fernandez-Medarde, A.; Santos, E. Ras in cancer and developmental diseases. *Genes Cancer* **2011,** *2* (3), 344-358.

2. Vigil, D.; Cherfils, J.; Rossman, K. L.; Der, C. J. Ras superfamily GEFs and GAPs: validated and tractable targets for cancer therapy? *Nat Rev Cancer* **2010,** *10* (12), 842-857.

3. Bos, J. L. Ras oncogenes in human cancer: a review. *Cancer Res* **1989,** *49* (17), 4682-4689.

4. Rodriguez-Viciana, P.; Sabatier, C.; McCormick, F. Signaling specificity by Ras family

GTPases is determined by the full spectrum of effectors they regulate. *Mol Cell Biol* **2004,** *24* (11), 4943-4954.

5. Malumbres, M.; Barbacid, M. RAS oncogenes: the first 30 years. *Nat Rev Cancer* **2003,** *3* (6), 459-465.

6. Mandala, M.; Merelli, B.; Massi, D. Nras in melanoma: targeting the undruggable target. *Crit Rev Oncol Hematol* **2014,** *92* (2), 107-122.

7. Karnoub, A. E.; Weinberg, R. A. Ras oncogenes: split personalities. *Nat Rev Mol Cell Biol* **2008,** *9* (7), 517-531.

8. Cicenas, J.; Tamosaitis, L.; Kvederaviciute, K.; Tarvydas, R.; Staniute, G.; Kalyan, K.; Meskinyte-Kausiliene, E.; Stankevicius, V.; Valius, M. KRAS, NRAS and BRAF mutations in colorectal cancer and melanoma. *Med Oncol* **2017,** *34* (2), 26.

9. Drosten, M.; Dhawahir, A.; Sum, E. Y. M.; Urosevic, J.; Lechuga, C. G.; Esteban, L. M.; Castellano, E.; Guerra, C.; Santos, E.; Barbacid, M. Genetic analysis of Ras signalling pathways in cell proliferation, migration and survival. *EMBO J* **2010,** *29* (6), 1091-1104.

10. Kelleher, F. C.; McArthur, G. A. Targeting NRAS in melanoma. *Cancer J* **2012,** *18* (2), 132-136.

11. Cogoi, S.; Xodo, L. E. G4 DNA in ras genes and its potential in cancer therapy. *Biochim Biophys Acta* **2016,** *1859* (4), 663-674.

12. Kumari, S.; Bugaut, A.; Huppert, J. L.; Balasubramanian, S. An RNA G-quadruplex in the 5' UTR of the NRAS proto-oncogene modulates translation. *Nat Chem Biol* **2007,** *3* (4), 218-221.

13. Kumari, S.; Bugaut, A.; Balasubramanian, S. Position and stability are determining

factors for translation repression by an RNA G-quadruplex-forming sequence within the 5' UTR of the NRAS proto-oncogene. *Biochemistry* **2008,** *47* (48), 12664-12669.

14. Bugaut, A.; Rodriguez, R.; Kumari, S.; Hsu, S. T.; Balasubramanian, S. Small molecule-mediated inhibition of translation by targeting a native RNA G-quadruplex. *Org Biomol Chem* **2010,** *8* (12), 2771-2776.

15. Bugaut, A.; Balasubramanian, S. 5'-UTR RNA G-quadruplexes: translation regulation and targeting. *Nucleic Acids Res* **2012,** *40* (11), 4727-4741.

16. Johnson, J. E.; Cao, K.; Ryvkin, P.; Wang, L. S.; Johnson, F. B. Altered gene expression in the Werner and Bloom syndromes is associated with sequences having G-quadruplex forming potential. *Nucleic Acids Res* **2010,** *38* (4), 1114-1122.

17. Chauhan, A.; Paul, R.; Debnath, M.; Bessi, I.; Mandal, S.; Schwalbe, H.; Dash, J. Synthesis of fluorescent binaphthyl amines that bind c-MYC G-quadruplex DNA and repress c-MYC expression. *J Med Chem* **2016,** *59* (15), 7275-7281.

18. Debnath, M.; Ghosh, S.; Chauhan, A.; Paul, R.; Bhattacharyya, K.; Dash, J. Preferential targeting of i-motifs and G-quadruplexes by small molecules. *Chem Sci* **2017,** *8* (11), 7448-7456.

19. Brown, R. V.; Wang, T.; Chappeta, V. R.; Wu, G.; Onel, B.; Chawla, R.; Quijada, H.; Camp, S. M.; Chiang, E. T.; Lassiter, Q. R.; Lee, C.; Phanse, S.; Turnidge, M. A.; Zhao, P.; Garcia, J. G. N.; Gokhale, V.; Yang, D.; Hurley, L. H. The consequences of overlapping g-quadruplexes and i-motifs in the platelet-derived growth factor receptor beta core promoter nuclease hypersensitive element can explain the unexpected effects of mutations and provide opportunities for selective targeting of both structures by small molecules to downregulate

gene expression. *J Am Chem Soc* **2017,** *139* (22), 7456-7475.

20. Kaiser, C. E.; Van Ert, N. A.; Agrawal, P.; Chawla, R.; Yang, D.; Hurley, L. H. Insight into the complexity of the i-Motif and G-quadruplex DNA structures formed in the KRAS promoter and subsequent drug-induced gene repression. *J Am Chem Soc* **2017,** *139* (25), 8522-8536.

21. Guilbaud, G.; Murat, P.; Recolin, B.; Campbell, B. C.; Maiter, A.; Sale, J. E.; Balasubramanian, S. Local epigenetic reprogramming induced by G-quadruplex ligands. *Nat Chem* **2017,** *9* (11), 1110-1117.

22. Xu, H.; Di Antonio, M.; McKinney, S.; Mathew, V.; Ho, B.; O'Neil, N. J.; Santos, N. D.; Silvester, J.; Wei, V.; Garcia, J.; Kabeer, F.; Lai, D.; Soriano, P.; Banath, J.; Chiu, D. S.; Yap, D.; Le, D. D.; Ye, F. B.; Zhang, A.; Thu, K.; Soong, J.; Lin, S. C.; Tsai, A. H.; Osako, T.; Algara, T.; Saunders, D. N.; Wong, J.; Xian, J.; Bally, M. B.; Brenton, J. D.; Brown, G. W.; Shah, S. P.; Cescon, D.; Mak, T. W.; Caldas, C.; Stirling, P. C.; Hieter, P.; Balasubramanian, S.; Aparicio, S. CX-5461 is a DNA G-quadruplex stabilizer with selective lethality in BRCA1/2 deficient tumours. *Nat Commun* **2017,** *8*, 14432.

23. Zhou, J. L.; Lu, Y. J.; Ou, T. M.; Zhou, J. M.; Huang, Z. S.; Zhu, X. F.; Du, C. J.; Bu, X. Z.; Ma, L.; Gu, L. Q.; Li, Y. M.; Chan, A. S. Synthesis and evaluation of quindoline derivatives as G-quadruplex inducing and stabilizing ligands and potential inhibitors of telomerase. *J Med Chem* **2005,** *48* (23), 7315-7321.

24. Ou, T. M.; Lu, Y. J.; Zhang, C.; Huang, Z. S.; Wang, X. D.; Tan, J. H.; Chen, Y.; Ma, D. L.; Wong, K. Y.; Tang, J. C.; Chan, A. S.; Gu, L. Q. Stabilization of G-quadruplex DNA and down-regulation of oncogene c-myc by quindoline derivatives. *J Med Chem* **2007,** *50* (7),

1465-1474.

25. Lu, Y. J.; Ou, T. M.; Tan, J. H.; Hou, J. Q.; Shao, W. Y.; Peng, D.; Sun, N.; Wang, X. D.; Wu, W. B.; Bu, X. Z.; Huang, Z. S.; Ma, D. L.; Wong, K. Y.; Gu, L. Q. 5-N-methylated quindoline derivatives as telomeric g-quadruplex stabilizing ligands: effects of 5-N positive charge on quadruplex binding affinity and cell proliferation. *J Med Chem* **2008,** *51* (20), 6381-6392.

26. Wang, X. D.; Ou, T. M.; Lu, Y. J.; Li, Z.; Xu, Z.; Xi, C.; Tan, J. H.; Huang, S. L.; An, L. K.; Li, D.; Gu, L. Q.; Huang, Z. S. Turning off transcription of the bcl-2 gene by stabilizing the bcl-2 promoter quadruplex with quindoline derivatives. *J Med Chem* **2010,** *53* (11), 4390-4398.

27. Ou, T. M.; Lin, J.; Lu, Y. J.; Hou, J. Q.; Tan, J. H.; Chen, S. H.; Li, Z.; Li, Y. P.; Li, D.; Gu, L. Q.; Huang, Z. S. Inhibition of cell proliferation by quindoline derivative (SYUIQ-05) through its preferential interaction with c-myc promoter G-quadruplex. *J Med Chem* **2011,** *54* (16), 5671-5679.

28. Long, Y.; Li, Z.; Tan, J. H.; Ou, T. M.; Li, D.; Gu, L. Q.; Huang, Z. S. Benzofuroquinoline derivatives had remarkable improvement of their selectivity for telomeric G-quadruplex DNA over duplex DNA upon introduction of peptidyl group. *Bioconjug Chem* **2012,** *23* (9), 1821-1831.

29. Wu, Y.; Zan, L. P.; Wang, X. D.; Lu, Y. J.; Ou, T. M.; Lin, J.; Huang, Z. S.; Gu, L. Q. Stabilization of VEGF G-quadruplex and inhibition of angiogenesis by quindoline derivatives. *Biochim Biophys Acta* **2014,** *1840* (9), 2970-2977.

30. Zeng, D. Y.; Kuang, G. T.; Wang, S. K.; Peng, W.; Lin, S. L.; Zhang, Q.; Su, X. X.; Hu,

M. H.; Wang, H.; Tan, J. H.; Huang, Z. S.; Gu, L. Q.; Ou, T. M. Discovery of novel 11-triazole substituted benzofuro[3,2-b]quinolone derivatives as c-myc G-quadruplex specific stabilizers via click chemistry. *J Med Chem* **2017,** *60* (13), 5407-5423.

31. Liu, H. Y.; Chen, A. C.; Yin, Q. K.; Li, Z.; Huang, S. M.; Du, G.; He, J. H.; Zan, L. P.; Wang, S. K.; Xu, Y. H.; Tan, J. H.; Ou, T. M.; Li, D.; Gu, L. Q.; Huang, Z. S. New disubstituted quindoline derivatives inhibiting Burkitt's lymphoma cell proliferation by impeding c-MYC transcription. *J Med Chem* **2017,** *60* (13), 5438-5454.

32. Wu, H.; Alexander, S. C.; Jin, S.; Devaraj, N. K. A bioorthogonal near-infrared fluorogenic probe for mRNA detection. *J Am Chem Soc* **2016,** *138* (36), 11429-11432.

33. Song, G.; Sun, Y.; Liu, Y.; Wang, X.; Chen, M.; Miao, F.; Zhang, W.; Yu, X.; Jin, J. Low molecular weight fluorescent probes with good photostability for imaging RNA-rich nucleolus and RNA in cytoplasm in living cells. *Biomaterials* **2014,** *35* (7), 2103-2112.

34. Lu, Y. J.; Deng, Q.; Hu, D. P.; Wang, Z. Y.; Huang, B. H.; Du, Z. Y.; Fang, Y. X.; Wong, W. L.; Zhang, K.; Chow, C. F. A molecular fluorescent dye for specific staining and imaging of RNA in live cells: a novel ligand integration from classical thiazole orange and styryl compounds. *Chem Commun (Camb)* **2015,** *51* (83), 15241-15244.

35. Liu, Y.; Zhang, W.; Sun, Y.; Song, G.; Miao, F.; Guo, F.; Tian, M.; Yu, X.; Sun, J. Z. Two-photon fluorescence imaging of RNA in nucleoli and cytoplasm in living cells based on low molecular weight probes. *Dyes Pigments* **2014,** *103*, 191-201.

36. Li, Q.; Kim, Y.; Namm, J.; Kulkarni, A.; Rosania, G. R.; Ahn, Y. H.; Chang, Y. T. RNA-selective, live cell imaging probes for studying nuclear structure and function. *Chem Biol* **2006,** *13* (6), 615-623.

37. Li, Q.; Chang, Y. T. A protocol for preparing, characterizing and using three RNA-specific, live cell imaging probes: E36, E144 and F22. *Nat Protoc* **2006,** *1* (6), 2922-2932.

38. Jin, M.; Xie, J.; Malval, J.-P.; Spangenberg, A.; Soppera, O.; Versace, D.-L.; Leclerc, T.; Pan, H.; Wan, D.; Pu, H.; Baldeck, P.; Poizat, O.; Knopf, S. Two-photon lithography in visible and NIR ranges using multibranched-based sensitizers for efficient acid generation. *J Mater Chem C* **2014,** *2* (35), 7201.

39. Feng, S.; Kim, Y. K.; Yang, S.; Chang, Y. T. Discovery of a green DNA probe for live-cell imaging. *Chem Commun (Camb)* **2010,** *46* (3), 436-438.

40. Wright, C. W.; Addae-Kyereme, J.; Breen, A. G.; Brown, J. E.; Cox, M. F.; Croft, S. L.; Gokcek, Y.; Kendrick, H.; Phillips, R. M.; Pollet, P. L. Synthesis and evaluation of cryptolepine analogues for their potential as new antimalarial agents. *J Med Chem* **2001,** *44* (19), 3187-3194.

41. Wang, Z.; Liu, D.; Cui, D. Statistically syndioselective coordination (Co)polymerization of 4-methylthiostyrene. *Macromolecules* **2016,** *49* (3), 781-787.

42. Pandey, A. K.; Sharma, R.; Shivahare, R.; Arora, A.; Rastogi, N.; Gupta, S.; Chauhan, P. M. S. Synthesis of perspicamide A and related diverse analogues: their bioevaluation as potent antileishmanial agents. *J Org Chem* **2013,** *78* (4), 1534-1546.

43. Kwong, L. N.; Costello, J. C.; Liu, H.; Jiang, S.; Helms, T. L.; Langsdorf, A. E.; Jakubosky, D.; Genovese, G.; Muller, F. L.; Jeong, J. H.; Bender, R. P.; Chu, G. C.; Flaherty, K. T.; Wargo, J. A.; Collins, J. J.; Chin, L. Oncogenic NRAS signaling differentially regulates survival and proliferation in melanoma. *Nat Med* **2012,** *18* (10), 1503-1510.

44. Schick, U.; Kyula, J.; Barker, H.; Patel, R.; Zaidi, S.; Gregory, C.; Hafsi, H.; Roulstone, V.; Deutsch, E.; McLaughlin, M.; Harrington, K. Trametinib radiosensitises RAS- and BRAF-mutated melanoma by perturbing cell cycle and inducing senescence. *Radiother Oncol* **2015,** *117* (2), 364-375.

45. Greger, J. G.; Eastman, S. D.; Zhang, V.; Bleam, M. R.; Hughes, A. M.; Smitheman, K. N.; Dickerson, S. H.; Laquerre, S. G.; Liu, L.; Gilmer, T. M. Combinations of BRAF, MEK, and PI3K/mTOR inhibitors overcome acquired resistance to the BRAF inhibitor GSK2118436 Dabrafenib, mediated by NRAS or MEK mutations. *Mol Cancer Ther* **2012,** *11* (4), 909-920.

46. Lipinski, C. A.; Lombardo, F.; Dominy, B. W.; Feeney, P. J. Experimental and computational approaches to estimate solubility and permeability in drug discovery and development settings. *Adv Drug Deliv Rev* **2001,** *46* (1-3), 3-26.

47. Allenmark, S. Induced circular dichroism by chiral molecular interaction. *Chirality* **2003,** *15* (409), 409-422.

48. Brazda, V.; Haronikova, L.; Liao, J. C.; Fojta, M. DNA and RNA quadruplex-binding proteins. *Int J Mol Sci* **2014,** *15* (10), 17493-17517.

49. Budhathoki, J. B.; Ray, S.; Urban, V.; Janscak, P.; Yodh, J. G.; Balci, H. RecQ-core of BLM unfolds telomeric G-quadruplex in the absence of ATP. *Nucleic Acids Res* **2014,** *42* (18), 11528-11545.

50. Wu, C. G.; Spies, M. G-quadruplex recognition and remodeling by the FANCJ helicase. *Nucleic Acids Res* **2016,** *44* (18), 8742-8753.

51. Vaughn, J. P.; Creacy, S. D.; Routh, E. D.; Joyner-Butt, C.; Jenkins, G. S.; Pauli, S.;

Nagamine, Y.; Akman, S. A. The DEXH protein product of the DHX36 gene is the major source of tetramolecular quadruplex G4-DNA resolving activity in HeLa cell lysates. *J Biol Chem* **2005,** *280* (46), 38117-38120.

52. Paeschke, K.; Bochman, M. L.; Garcia, P. D.; Cejka, P.; Friedman, K. L.; Kowalczykowski, S. C.; Zakian, V. A. Pif1 family helicases suppress genome instability at G-quadruplex motifs. *Nature* **2013,** *497* (7450), 458-462.

53. Sexton, A. N.; Collins, K. The 5' guanosine tracts of human telomerase RNA are recognized by the G-quadruplex binding domain of the RNA helicase DHX36 and function to increase RNA accumulation. *Mol Cell Biol* **2011,** *31* (4), 736-743.

54. Chen, M. C.; Murat, P.; Abecassis, K.; Ferre-D'Amare, A. R.; Balasubramanian, S. Insights into the mechanism of a G-quadruplex-unwinding DEAH-box helicase. *Nucleic Acids Res* **2015,** *43* (4), 2223-2231.

55. Yangyuoru, P. M.; Bradburn, D. A.; Liu, Z.; Xiao, T. S.; Russell, R. The G-quadruplex (G4) resolvase DHX36 efficiently and specifically disrupts DNA G4s via a translocation-based helicase mechanism. *J Biol Chem* **2018,** *293* (6), 1924-1932.

56. Newman, M.; Sfaxi, R.; Saha, A.; Monchaud, D.; Teulade-Fichou, M. P.; Vagner, S. The G-quadruplex-specific RNA helicase DHX36 regulates p53 pre-mRNA 3'-end processing following UV-Induced DNA damage. *J Mol Biol* **2017,** *429* (21), 3121-3131.

57. Booy, E. P.; Howard, R.; Marushchak, O.; Ariyo, E. O.; Meier, M.; Novakowski, S. K.; Deo, S. R.; Dzananovic, E.; Stetefeld, J.; McKenna, S. A. The RNA helicase RHAU (DHX36) suppresses expression of the transcription factor PITX1. *Nucleic Acids Res* **2014,** *42* (5), 3346-3361.

58. Creacy, S. D.; Routh, E. D.; Iwamoto, F.; Nagamine, Y.; Akman, S. A.; Vaughn, J. P. G4 resolvase 1 binds both DNA and RNA tetramolecular quadruplex with high affinity and is the major source of tetramolecular quadruplex G4-DNA and G4-RNA resolving activity in HeLa cell lysates. *J Biol Chem* **2008,** *283* (50), 34626-34634.

59. Vagelli, D.; Kiaris, H.; Delakas, D.; Anezinis, P.; Cranidis, A.; Spandidos, D. A. Transcriptional activation of H-ras, K-ras and N-ras proto-oncogenes in human bladder tumors. *Cancer Lett* **1996,** *107*, 241-247.

■ SCHEME AND FIGURES LEGENDS

Scheme 1. Synthesis of the **MSQ** derivatives. Reagents and conditions: (i) *4*-(methylthio) styryl, palladium acetate, P(o-tol)$_3$, anhydrous THF, anhydrous Et_3N, 110 ^oC, 40 h; (ii) PTSA, different amino side chains, 120 ^oC, 16-24 h; (iii) CH_3I, tetramethylene sulfone, 68 ^oC, 48 h; (v) 2-ethoxyethanol, different amino side chains, 120 ^oC, 24 h.

Figure 1. Modification strategies of the **MSQ** derivatives and structures of these derivatives.

Figure 2. Results from the SPR screening assay. The biotin-NRQ, biotin-NRQ_mutant, and biotin-hairpin were immobilized in flow cells. All the **MSQ** compounds were diluted with a running buffer (50 mM Tris-HCl, 150 mM KCl, 0.005% Tween-20) from stock solutions to final concentrations. The compounds flowed for 180 s during the association phase followed by a 300-s disassociation phase. The dissociating constants (K_D) between the oligomers and the compounds were analyzed by the ProteOn® manager software, using an equilibrium model to fit the kinetic data: K_D = ([A]×[B]) / [AB]. Here, [AB] is the concentration of the complex, [A] and [B] are the concentrations of analyte and the substance, respectively. Insets below the histogram showed the scaffolds of each series. Compounds with no specific binding to the NRQ oligomer were excluded from the histogram.

Figure 3. The IC_{50} of the **MSQ** derivatives on proliferation of human melanoma cells A375, human lung adenocarcinoma cells A549, human cervical cancer cells Hela, human hepatoma cells Huh7, human colon cancer cells HCT116, human breast cancer cells MCF-7, and human normal colon mucosal epithelial cells NCM460. The active strength of these compounds is marked by gradient color, in which deep red represents the lowest IC_{50} value while deep blue represents the highest IC_{50} value. The experiments were repeated separately for three times.

Figure 4. (a) Plots of IC_{50} values of each compounds for A375 cells plotted as an effect of the binding of compounds to the *NRAS* G-quadruplex. **(b)** Radar chart for the physiochemical properties of **4a-10** (violet) and **4a-16** (yellow). The green shaded area indicates the optimum range for each feature. *n*OHNH, number of hydrogen bond donors (≤5); *n*ON, number of hydrogen bond acceptors (≤5); Mw, molecular mass (≤500 Da); PSA, polar surface area (≤50 $Å^2$); clogD, partition coefficient (≤5).

Figure 5. (a) and **(b),** SPR sensorgrams of the NRQ oligomer in the addition with compound **4a-10** (**a**) and **4a-16** (**b**) at increasing concentrations. **(c)** and **(d),** UV-vis spectrum of **4a-10 (c)** and **4a-16 (d)** when titrated with the NRQ oligomer in a 10 mM Tris-HCl buffer (pH 7.4) containing 100 mM KCl. Arrows indicated the increasing concentration of the NRQ oligomer. The insets showed the Sigmoidal fitting curve using the absorption at 435 nm and the calculated K_D values.

Figure 6. Results of the CD-melting experiments. 5 μM of the NRQ oligomer was

incubated with 5 μM **4a-10 (b)**, 5 μM **4a-16 (c)**, or 10 μM **4a-10 (d)** in a 10 mM Tris-HCl buffer (pH 7.4, 200 μM KCl) followed by an annealing process. The spectrum was recorded with an interval of 5 ^{o}C. The insets showed melting curves and T_m values using the CD signals at 264 nm.

Figure 7. Western blot results of the NRAS protein from A375 cells treated with **4a-10** (**a**) or **4a-16** (**b**) at increasing concentrations for 6 h or treated with 1 μM **4a-10** (**c**) or **4a-16** (**d**) and collected cells from different time points. GAPDH was used as an internal control.

Figure 8. (a) and **(b),** The transcription of *NRAS* gene in A375 cells treated with **4a-10** for 6 h by using the qRT-PCR. *β-actin* gene was used as the internal control. The amounts of *NRAS* transcripts were calculated by the standard $2^{-\Delta\Delta Ct}$ method and were made as a histogram (**b**). # P > 0.05. **(c)** Western blot results of the NRAS protein from MCF-7 cells treated with **4a-10** at increasing concentrations for 6 h. GAPDH was used as an internal control. **(d)** and **(e)** The effects of **4a-10** on *NRAS* 5'-UTR activity by using the dual luciferase reporter assay. Column graph shows the relative expression level of the *Renilla* luciferase (activity of *Renilla* luciferase/activity of *Firefly* luciferase) in plasmids containing wild-type (**d**) or mutant *NRAS* 5'-UTR (**e**) after the addition of **4a-10** at 0.125 μM, 0.25 μM, and 0.5 μM. ***P<0.0005, *P<0.05, #P>0.05. **(f)** RT-PCR results of *NRAS* 5'-UTR from a RIP assay with DHX36 antibody treated without or with 2-μM **4a-10**. IgG was used

as a negative control.

Figure 9. (a) Cell cycle analysis of A375 cells treated with **4a-10** (0.125, 0.25, and 0.5μM) after propidium iodide (PI) staining. **(b)** The percentage of cells in different phases of the cell cycle. **(c)** A375 cells were treated with 0.25 μM **4a-10** for 6 h and fixed with 4% polyoxymethylene. Then, cells were incubated with DAPI for 15 min in dark. Fluorescent images of **4a-10** (red) and DAPI (blue) were obtained using a FV3000 laser scanning confocal microscope with a 600 magnification times.

■ TABLE OF CONTENTS GRAPHIC

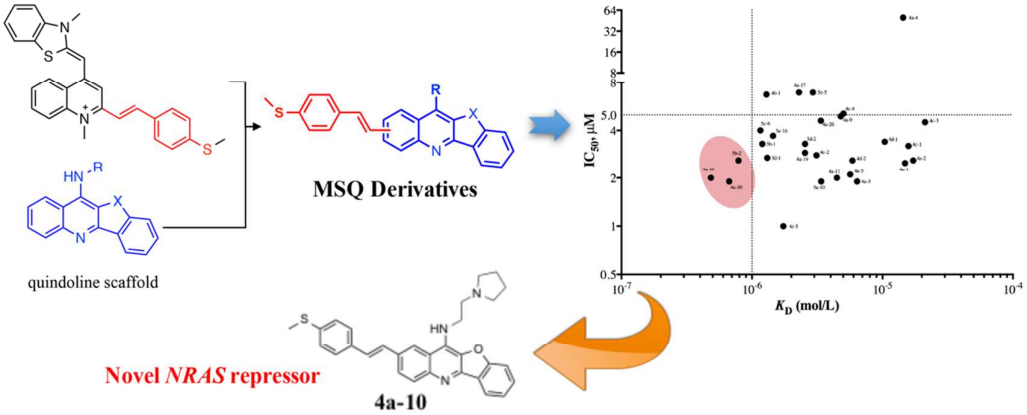

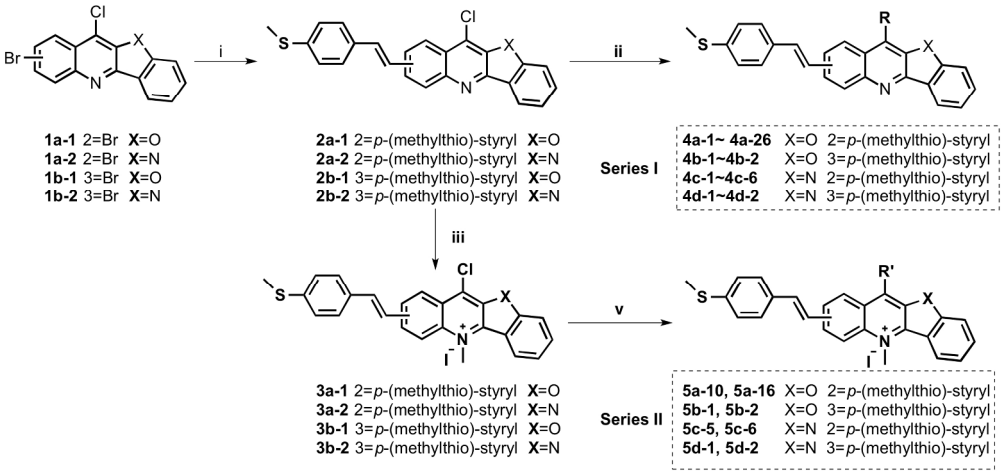

Scheme 1. Synthesis of the MSQ derivatives. Reagents and conditions: (i) 4-(methylthio) styryl, palladium acetate, P(o-tol)3, anhydrous THF, anhydrous Et3N, 110 oC, 40 h; (ii) PTSA, different amino side chains, 120 oC, 16-24 h; (iii) CH3I, tetramethylene sulfone, 68 oC, 48 h; (v) 2-ethoxyethanol, different amino side chains, 120 oC, 24 h.

216x102mm (300 x 300 DPI)

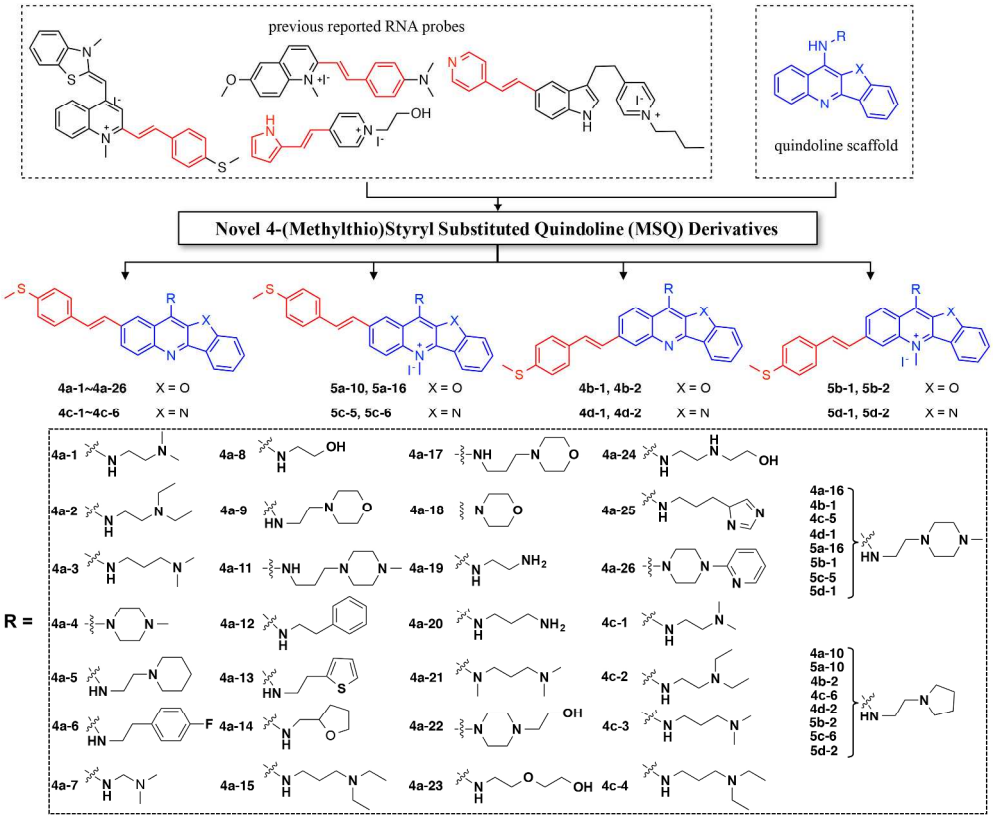

Figure 1. Modification strategies of the MSQ derivatives and structures of these derivatives.

264x214mm (300 x 300 DPI)

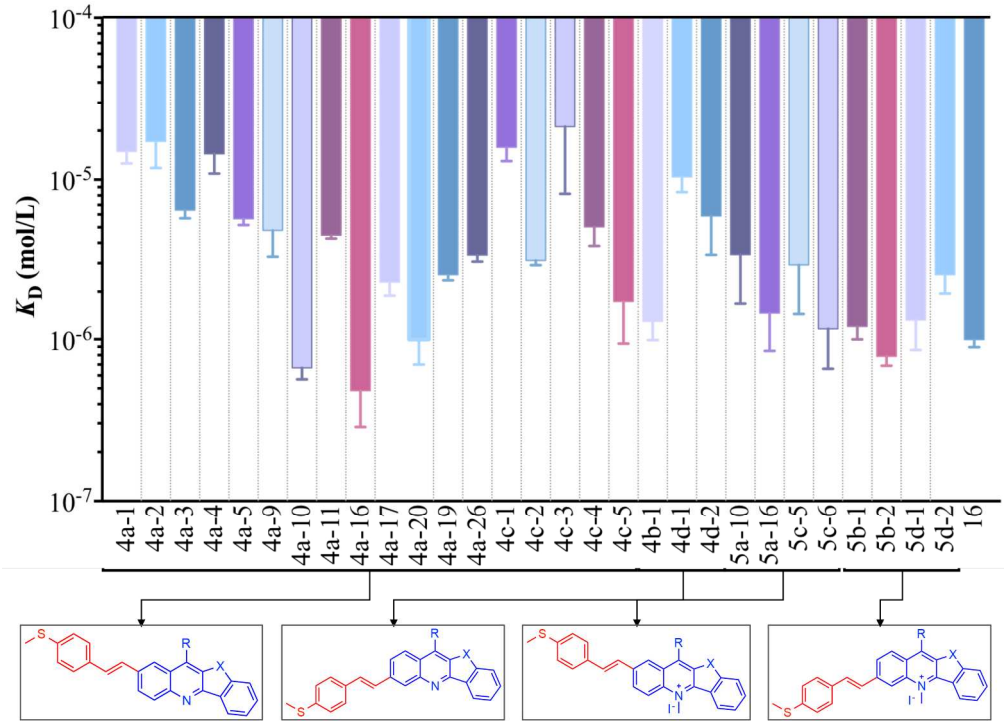

Figure 2. Results from the SPR screening assay. The biotin-NRQ, biotin-NRQ_mutant, and biotin-hairpin were immobilized in flow cells. All the MSQ compounds were diluted with a running buffer (50 mM Tris-HCl, 150 mM KCl, 0.005% Tween-20) from stock solutions to final concentrations. The compounds flowed for 180 s during the association phase followed by a 300-s disassociation phase. The dissociating constants (KD) between the oligomers and the compounds were analyzed by the ProteOn® manager software, using an equilibrium model to fit the kinetic data: KD = ([A]×[B]) / [AB]. Here, [AB] is the concentration of the complex, [A] and [B] are the concentrations of analyte and the substance, respectively. Insets below the histogram showed the scaffolds of each series. Compounds with no specific binding to the NRQ oligomer were excluded from the histogram.

209x150mm (300 x 300 DPI)

	A375	A549	Hela	Huh7	HCT116	MCF-7	NCM460
4a-1	2.5	2.8	3.3	1.7	6.0	2.9	15.6
4a-2	2.6	2.4	1.8	1.7	4.8	2.8	7.4
4a-3	1.9	2.5	2.6	2.0	5.3	4.4	5.6
4a-4	50.0	50.0	50.0	50.0	50.0	50.0	50.0
4a-5	2.1	24.1	6.7	7.8	10.5	3.8	17.0
4a-6	50.0	50.0	50.0	50.0	50.0	50.0	50.0
4a-7	29.1	40.6	18.5	41.5	50.0	50.0	50.0
4a-8	42.8	50.0	50.0	50.0	50.0	50.0	50.0
4a-9	4.9	2.8	3.3	5.0	24.9	27.6	50.0
4a-10	1.9	1.1	1.0	1.7	1.6	1.5	8.8
4a-11	2.0	5.2	4.2	4.9	1.7	14.9	50.0
4a-12	50.0	50.0	50.0	50.0	50.0	50.0	50.0
4a-13	50.0	50.0	50.0	50.0	50.0	50.0	50.0
4a-14	2.2	50.0	6.1	8.3	15.7	24.1	50.0
4a-15	2.8	3.0	3.0	1.9	5.1	1.5	5.2
4a-16	2.0	2.0	1.7	3.2	4.4	2.3	10.0
4a-17	6.9	7.0	5.0	7.0	43.9	34.0	50.0
4a-18	50.0	50.0	50.0	40.2	50.0	50.0	50.0
4a-19	2.9	2.7	4.7	1.9	5.1	4.5	19.6
4a-20	2.4	1.8	2.9	1.5	2.4	1.2	3.4
4a-21	4.2	2.8	3.1	2.9	4.4	3.5	8.2
4a-22	50.0	50.0	50.0	50.0	50.0	50.0	50.0
4a-23	9.6	35.8	8.4	9.5	50.0	13.4	50.0
4a-24	6.6	4.3	3.5	5.8	19.4	20.1	48.8
4a-25	50.0	50.0	50.0	50.0	50.0	50.0	50.0
4a-26	4.6	11.3	5.0	5.8	26.7	5.3	13.2
4b-1	6.7	1.5	1.9	2.1	2.7	4.0	17.2
4b-2	5.8	4.7	5.1	1.8	2.9	50.0	50.0
4c-1	3.2	2.8	2.0	2.1	4.0	5.1	10.2
4c-2	2.8	2.0	2.3	2.3	3.2	6.2	12.2
4c-3	4.5	3.1	2.7	2.0	3.8	8.0	16.1
4c-4	5.1	4.2	2.0	3.2	2.7	7.2	15.6
4c-5	1.0	2.6	1.9	1.1	2.4	3.3	3.0
4c-6	4.5	4.3	3.9	4.8	6.5	50.0	5.6
4d-1	3.4	6.3	1.4	1.7	1.8	6.2	14.2
4d-2	2.6	9.8	1.2	1.4	1.2	2.7	10.2
5a-10	2.5	3.2	2.1	4.5	5.3	3.7	11.6
5a-16	3.7	4.8	4.9	1.5	2.3	1.2	7.0
5b-1	3.3	3.7	1.9	0.5	1.3	2.1	2.8
5b-2	2.6	50.0	3.7	2.4	3.9	2.3	3.4
5c-5	6.9	4.3	2.0	4.7	5.4	6.6	6.2
5c-6	4.0	4.0	50.0	4.3	5.2	26.6	43.0
5d-1	2.7	3.0	2.1	4.0	4.3	1.7	3.0
5d-2	3.3	2.0	2.2	4.1	4.4	4.4	4.4

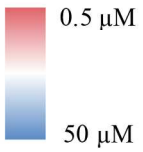

Figure 3. The IC50 of the MSQ derivatives on proliferation of human melanoma cells A375, human lung adenocarcinoma cells A549, human cervical cancer cells Hela, human hepatoma cells Huh7, human colon cancer cells HCT116, human breast cancer cells MCF-7, and human normal colon mucosal epithelial cells NCM460. The active strength of these compounds is marked by gradient color, in which deep red represents the lowest IC50 value while deep blue represents the highest IC50 value. The experiments were repeated separately for three times.

165x230mm (300 x 300 DPI)

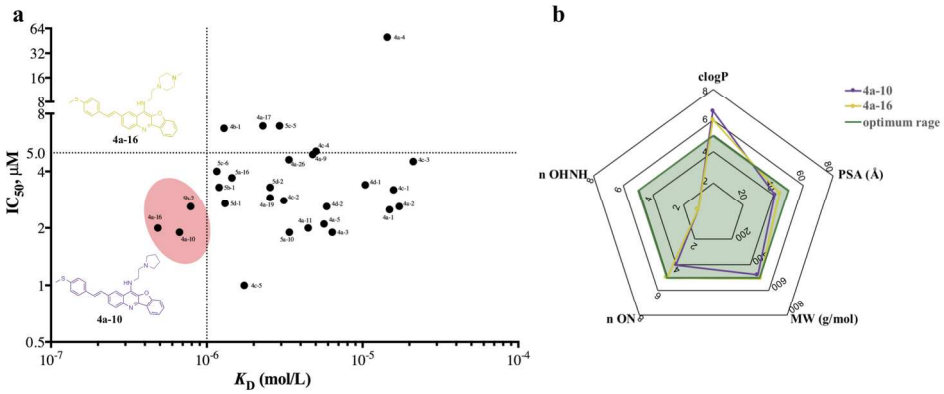

Figure 4. (a) Plots of IC50 values of each compounds for A375 cells plotted as an effect of the binding of compounds to the NRAS G-quadruplex. (b) Radar chart for the physiochemical properties of 4a-10 (violet) and 4a-16 (yellow). The green shaded area indicates the optimum range for each feature. n OHNH, number of hydrogen bond donors (≤5); n ON, number of hydrogen bond acceptors (≤5); Mw, molecular mass (≤500 Da); PSA, polar surface area (≤50 Å2); clogD, partition coefficient (≤5).

169x69mm (300 x 300 DPI)

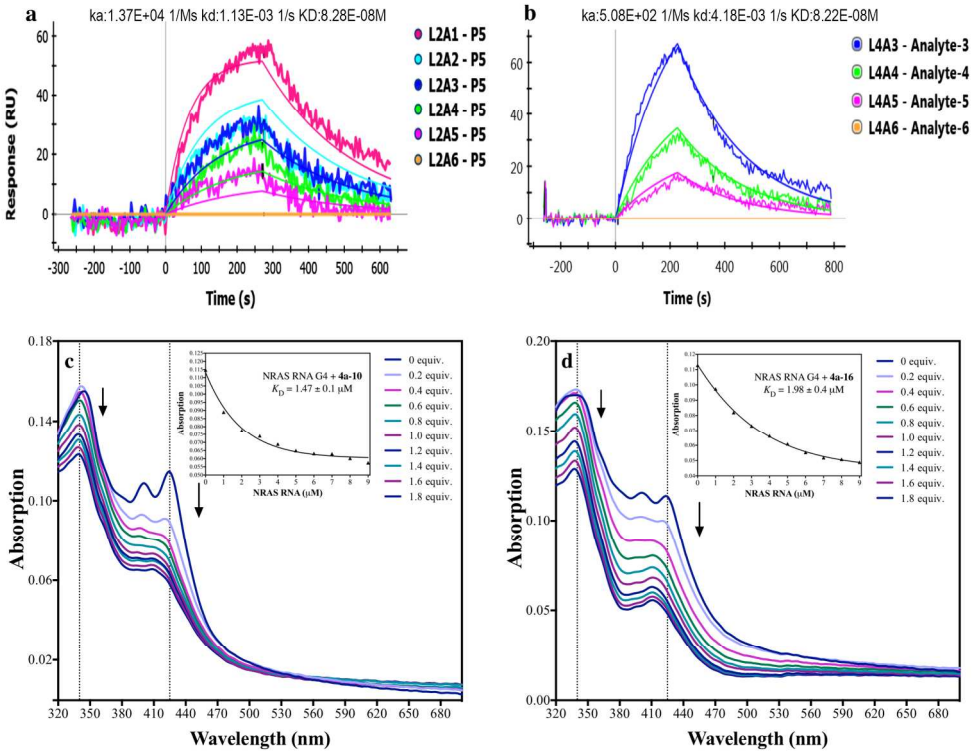

Figure 5. (a) and (b), SPR sensorgrams of the NRQ oligomer in the addition with compound 4a-10 (a) and 4a-16 (b) at increasing concentrations. (c) and (d), UV-vis spectrum of 4a-10 (c) and 4a-16 (d) when titrated with the NRQ oligomer in a 10 mM Tris-HCl buffer (pH 7.4) containing 100 mM KCl. Arrows indicated the increasing concentration of the NRQ oligomer. The insets showed the Sigmoidal fitting curve using the absorption at 435 nm and the calculated KD values.

195x145mm (300 x 300 DPI)

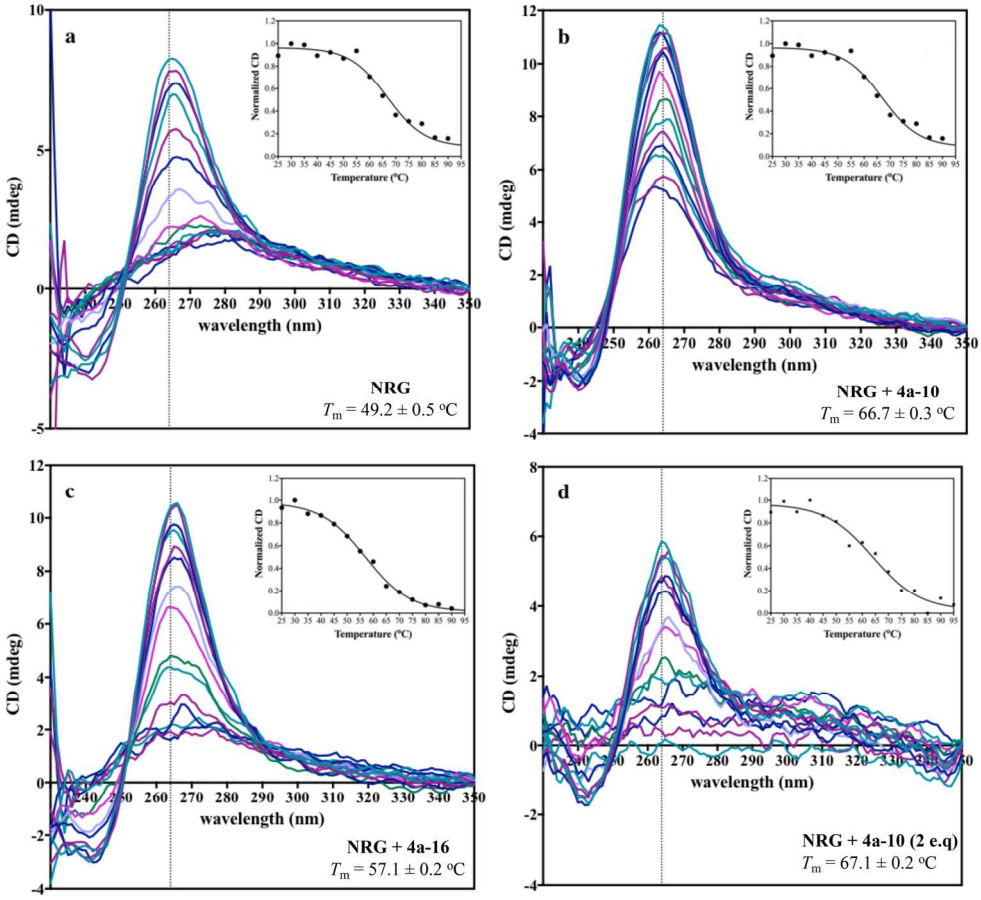

Figure 6. Results of the CD-melting experiments. 5 μM of the NRQ oligomer was incubated with 5 μM 4a-10 (b), 5 μM 4a-16 (c), or 10 μM 4a-10 (d) in a 10 mM Tris-HCl buffer (pH 7.4, 200 μM KCl) followed by an annealing process. The spectrum was recorded with an interval of 5 oC. The insets showed melting curves and Tm values using the CD signals at 264 nm.

190x174mm (300 x 300 DPI)

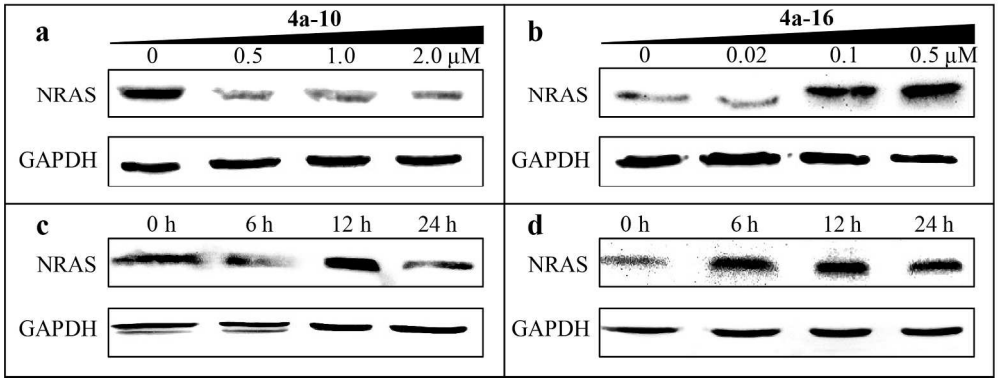

Figure 7. Western blot results of the NRAS protein from A375 cells treated with 4a-10 or 4a-16 with increasing concentration for 6 h (a) and (b), or treated with 1 μM 4a-10 or 4a-16 and collected cells from different time points (c) and (d). GAPDH was used as an internal control.

211x80mm (300 x 300 DPI)

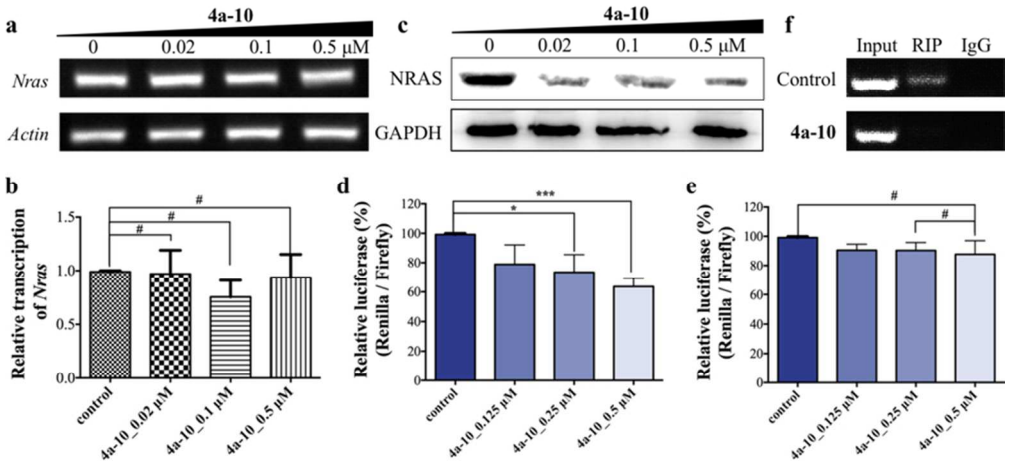

Figure 8. (a) and (b), The transcription of NRAS gene in A375 cells treated with 4a-10 for 6 h by using the qRT-PCR. β-actin gene was used as the internal control. The amounts of NRAS transcripts were calculated by the standard 2-ΔΔCt method and were made as a histogram (b). # P > 0.05. (c) Western blot results of the NRAS protein from MCF-7 cells treated with 4a-10 at increasing concentrations for 6 h. GAPDH was used as an internal control. (d) and (e) The effects of 4a-10 on NRAS 5′-UTR activity by using the dual luciferase reporter assay. Column graph shows the relative expression level of the Renilla luciferase (activity of Renilla luciferase/activity of Firefly luciferase) in plasmids containing wild-type (d) or mutant NRAS 5′-UTR (e) after the addition of 4a-10 at 0.125 μM, 0.25 μM, and 0.5 μM. ***P<0.0005, *P<0.05, #P>0.05. (f) RT-PCR results of NRAS 5′-UTR from a RIP assay with DHX36 antibody treated without or with 2-μM 4a-10. IgG was used as a negative control.

79x37mm (300 x 300 DPI)

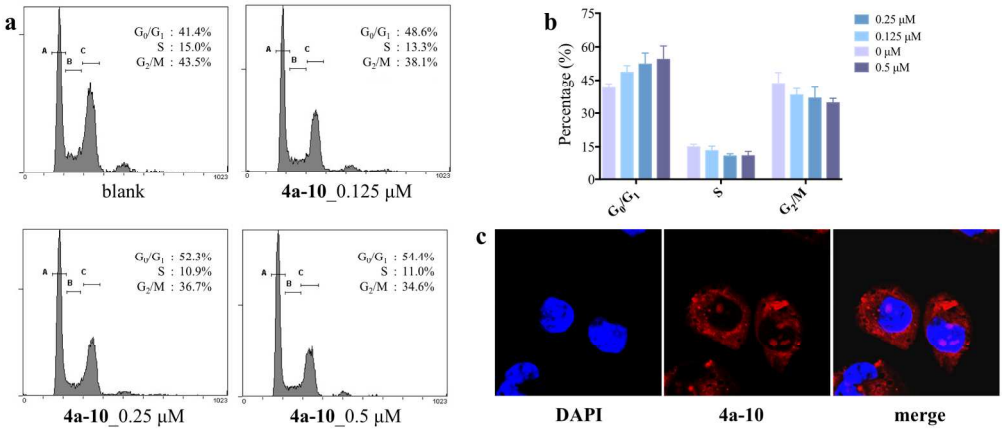

Figure 9. (a) Cell cycle analysis of A375 cells treated with 4a-10 (0.125, 0.25, and 0.5μM) after propidium iodide (PI) staining. (b) The percentage of cells in different phases of the cell cycle. (c) A375 cells were treated with 0.25 μM 4a-10 for 6 h and fixed with 4% polyoxymethylene. Then, cells were incubated with DAPI for 15 min in dark. Fluorescent images of 4a-10 (red) and DAPI (blue) were obtained using a FV3000 laser scanning confocal microscope with a 600 magnification times.

210x90mm (300 x 300 DPI)